Dynamic simulation and optimal operation of district cooling networks via 2D orthogonal collocation

Arley Nova-Rincon, Sabine Sochard, Sylvain Serra, Jean-Michel Reneaume

Dynamic Simulation and Optimal Operation of District Cooling Networks via 2D Orthogonal Collocation

Arley NOVA-RINCON[1*], Sabine SOCHARD[1], Sylvain SERRA[1], Jean-Michel RENEAUME[1].

[1] UNIV PAU & PAYS ADOUR/ E2S UPPA, LABORATOIRE DE THERMIQUE, ENERGETIQUE ET PROCEDES- IPRA, EA1932, 64000, PAU, FRANCE
[*](Corresponding author: arley.nova-rincon@univ-pau.fr)

Abstract

Due to the increasing demand for cooling worldwide and the need for reliable and energy-efficient alternatives to provide it, the analysis of district cooling (DC) networks has become a focus of interest in recent years. In DC networks, the temperature of the cooling utility returning to the production site must be close to the design temperature of the installed technology to ensure proper efficiency and avoid the technical issue known as low ΔT syndrome. Via dynamic optimisation, it is possible to compute the mass flow profiles in the network that lead to an operation which overcomes this problem. In this paper, we propose a methodology that provides a simultaneous (equation- oriented) solution to this dynamic optimisation problem using 2D Orthogonal Collocation on Finite Elements (OCFE). We apply this methodology to a medium-sized cooling system serving 20 consumers of different categories with fluctuating cooling demands subject to variable external conditions. The dynamic simulation and optimisation were performed using insulated and non-insulated piping. The proposed methodology exhibits low computational cost, demonstrating its potential use for developing applications for operating and forecasting these systems.

1 Introduction

Today, heating and cooling account for more than 50% of the total energy demand in Europe [1]. Furthermore, most of the energy used by this sector still comes from non-renewables, representing a major source of CO_2 emissions that needs to be urgently mitigated [2]. With this in mind, district energy systems are emerging as an interesting alternative to mitigate the environmental impact of these emissions [3]. Compared to individual heating and cooling, District Heating and Cooling (DHC) systems have higher efficiency, are more economically attractive for high demand buildings, could reduce fuel consumption, improve community energy management and allow better control of emissions [3].

There is a strong motivation to optimise district energy systems as they minimise the cost of infrastructure and emissions while maximizing the production of the hot or cold utility, and its efficiency. Such optimisation is particularly challenging because of technical characteristics and the

size of real-world applications [4]. In general, mathematical optimisation of these systems is very much skewed in favour of district heating systems, as stated by Werner [5]. However, despite the lack of analysis of district cooling systems, most of the methodologies applied to the analysis of district heating systems (DHS) can also be used to study district cooling systems. It is important to point out that each kind of system presents its own issues, related not only to the kind of utility produced (hot or cold) but also to the way it improves system efficiency, as will be detailed in the objectives of this work. Hence the importance of studies focused on district cooling networks.

Before introducing the applications for optimising district energy systems, it is important to present a general classification of the type of problems we find in mathematical optimisation. An optimisation problem consists of one (or sometimes more) objective function that has to be minimised (e.g. Operational cost, CO_2 emissions) or maximised (efficiency, production), subject to the fulfilment of the physical or operational constraints of the system, which are represented as equality or inequality constraints, by manipulating a set of decision variables. Depending on the nature of the decision variables (continuous or discrete), a general categorisation of optimisation problems can be established, which is independent of the methods implemented to solve the problem as stated by Biegler and Grossmann [6]. If the problem is described using only continuous variables when considering the nature of the constraints and the objective function that describes the system (linear or non-linear), we have linear programming (LP) and non-linear programming (NLP) problems. When discrete variables are involved, they are classified as mixed-integer linear programming (MILP) and mixed-integer non-linear programming (MINLP) problems. Finally, when dealing with dynamic models, two approaches are possible. Either we represent the dynamic problem as a succession of steady-state problems, known as multi-period optimisation, or we deal with the dynamics of the system. In the latter case, we can use either Pontryagin's principle (optimal control) or discretisation, formulating the dynamic problem as an algebraic problem (NLP, MILP or MINLP), known as dynamic optimisation.

According to the classification described above, we can organise studies on the optimisation of district heating and cooling as presented in Table 1. This detail selected contributions in terms of the kind of problem that is solved and their main applications (due to the complexity of the models used to describe these systems, there are few instances of LP applied to district heating and cooling, which is why no LP problem is reported). More extensive reviews on the applications of optimisation in District energy systems are presented by Talebi *et al.* [7], Sameti *et al.* [4], Gang *et al.* [8]. Eveloy and Ayou [9] also present optimisation applications specifically for DCS. They highlight the fact that most studies have focused on optimising distribution network infrastructure (the selection of technologies, the number and kinds of users connected to the network, the existence of network elements such as

pumps, chillers, storage tanks, pipes), considering steady-state models and leading to a MILP or MINLP formulation. On the other hand, one of the most unexplored subjects of study in the field of energy systems is the dynamic optimisation and control of these systems, as stated by Gang *et al.* [8] and Allegrini *et al.* [10].

Table 1. Classification of studies on DHC Optimisation

Continuous Variables	**Integer variables**	
NLP	**MILP**	**MINLP**
	Data based Chow *et al.* [11] - Diversity factor	**Data based** Deng *et al.* [12] - Scheduling
	Steady-State Söderman [13] - Topology - Operation (flow rates)	**Steady-State** Mertz *et al.* [14] Marty *et al.* [15] - Topology - Sizing - Operation
	Multiperiod Khir *et al.* [16] - Sizing - Topology - Operation	
Dynamic Schweiger *et al*. [17] - Operation (Modelica) This contribution - Operation (2D-OCFE)		**Data based MIQCP** Schweiger *et al*. [17] - Scheduling

Among the applications used in district cooling, some studies are based on data. Chow *et al.* [11] presented a MILP formulation that optimised the diversity factor, which is the proportion of diverse types of building (office, residential, shops, hotels and mass transit railway stations), resulting in a uniform cooling load to ensure a high stability in the cold production system to be installed. They first calculated typical 24-hour demand profiles for five types of building for 36 typical days (three typical days per month), using a freeware building energy analysis programme that can predict energy use and cost for all types of building. With these data, they then implemented a genetic algorithm to solve a MILP problem that aims to minimize a fluctuation index with respect to the maximum cooling demand. Here, the optimisation variables are the number of buildings for each of the five categories. In order to avoid local optimum, they used a genetic algorithm. However, their study does not consider the topology of the network, which could have a considerable impact on the delay and the formulation of the fluctuation index. Moving to MINLP applications, Deng *et al.* [12] presented an approach for the optimal scheduling of an actual DHC system that minimised its daily operation cost. The system was composed of an electric chiller system, a ground source heat pump, a thermal storage system and

a combined cooling, heating and power system. The nonlinearities of the continuous variables corresponded to the operational conditions of each of the components of the system, while the discrete variables corresponded to the use (on/off) of the chillers in different periods of energy demand. This contribution optimised the energy mixing of the system, aiming to cover a given total demand, but assumed that the equipment always operated at nominal levels. However, they did not consider the interactions of the clients with the distribution system nor their location with respect to the production site.

Continuing with steady-state studies, Söderman [13] presented an optimisation of the structure and operation of an existing cooling network, based on a steady-state model of the users' maximum cooling demand. He also presented a project in which the capacity of the network would be increased to serve almost twice as many customers. To expand the network, he computed the location of new energy storage and production sites, as well as the pipe connections of the new interconnected system. This work included the linearisation of the mathematical model of the network. The problems were solved using the MILP CPLEX solver. Although this contribution, contrary to the previous one, presented a detailed analysis of the network, some parameters (pipe diameters) were not reported. Also, the steady-state assumption could prevent the use of renewables to expand the network. Finally, the assumption of constant cooling demands could result in an overestimation of the production of cold. MINLP steady-state applications in heating networks are found in the works of Mertz *et al.* [14] and Marty *et al.* [15]. The former performed a combinatory non-linear optimisation to find the topology and substation exchanger size that minimised the global cost of a district heating network. The resulting MINLP problem was solved using DICOPT within GAMS®. Marty *et al.* [15] implemented a strategy to simultaneously optimise the district heating network topology, the Organic Rankine Cycle (ORC) sizing of a geothermal plant, and the distribution of the geothermal fluid between the ORC and the DHN. To solve the proposed MINLP problem, they used the MINLP DICOPT solver in the GAMS® environment. Since the main critical point in solving an MINLP problem is its initialisation, Mertz *et al.* [14] and Marty *et al.* [15] also presented their strategies to overcome this point. However, all of these studies were performed for steady-state conditions, although the variable customer demand, the thermal storage or, sometimes, the use of intermittent renewable energy result in the district heating and district cooling networks becoming dynamic systems.

The multiperiod application presented by Khir and Haouari [16] developed an approximation for the optimal design of a DCS whose results comprised the chiller plant size, storage tank size, layout of the network and the quantities of energy produced and stored during each period. They used the ILOG CPLEX software package, with the aim of minimising the amount of investment and the operational

cost of the system. District planning included studies on the influence of the number and kind of buildings served by the cooling network. Their model considers the demand of the user at each period but does not consider the dynamics of temperature in the system pipes.

As already stated, one of the least explored subjects of study in the field of energy systems is the dynamic optimisation and control of these systems.

Recent advances in this field include the study by Schweiger *et al.* [17] dealing with optimal production planning in district heating systems. They presented a framework to represent on-grid energy systems and performed a dynamic thermo-hydraulic simulation of energy systems. The framework was based on the Modelica® modelling language, performing the continuous optimisation tasks with the OPTIMICA compiler toolkit, and the discrete optimisation in the Python open-source environment using the Pyomo module. They decomposed the resulting mixed-integer-optimal control problem into a Mixed Integer Quadratic Constrained Programming (MIQCP) problem (a particular form of MINLP problem) and a continuous problem. The results of the former provided the status and heat production of each unit. The discrete variables representing the status of each unit were thus fixed by this solution from the MIQCP, although the real heat production was calculated in the continuous problem which was transformed into a Nonlinear Programming (NLP) problem using a direct collocation method, then solved using the interior point algorithm IPOPT. The objective function proposed in this work (and which had to be minimised) was the supply temperature of the producer for the duration of the considered time span. Although this implementation is based on physical models, it is fully tool-oriented to Modelica users, offering few details on the mathematical modelling and treatment of the dynamic optimisation problem. This fact makes it difficult to replicate their methodology on other available modelling and optimisation tools. In the field of the dynamic optimisation of energy systems, we can also mention the dynamic optimisation of a hybrid Solar thermal and fossil Fuel system [18].

To our knowledge, studies on the dynamic optimisation of district energy systems are limited to the aforementioned works. We hope to contribute to this field and propose a dynamic optimisation of the return temperature of a district cooling network. The choice of this objective function will be discussed later; we will first introduce the dynamic problems and the way they can be solved.

Dynamic optimisation has been used for off-line tasks, including studies on operation in response to disturbances. As proposed by Schweiger *et al.* [17] a general form for optimisation problems of this kind can be represented as:

$$\min_{z,y,u,par} J = \phi\left(t_f, z(t_f)\right) + \int_{t_0}^{t_f} \mathcal{L}(t,z,y,u)dt \tag{1}$$

$$s.t. \quad \frac{dz(t)}{dt} = f(t,z(t),y(t),u(t),par), \quad z(t_0) = z_0, \tag{2}$$

$$g(z(t),y(t),u(t),par) = 0, \tag{3}$$

$$g_f\left(z(t_f)\right) = 0, \tag{4}$$

$$u_L \leq u(t) \leq u_U, \qquad y_L \leq y(t) \leq z_y, \qquad z_L \leq z(t) \leq z_U \tag{5}$$

where $z(t)$ are the differential state variables, $y(t)$ the algebraic state variables, $u(t)$ the control variables, all of which are functions of time $t \in [t_0, t_f]$, and par represents the time-independent parameters. The constraints of this optimisation problem are the Differential and Algebraic Equations (DAE) (2)-(4). This formulation is known as the problem of Bolza [19], where J is a scalar to be minimised. The first term corresponds to the Mayer term and the integral term corresponds to the Lagrange term. Thus, depending on the application, in dynamic optimisation, it is possible to formulate objective functions of the form of Bolza, Mayer or Lagrange.

Biegler [20-21] reported different ways to solve the aforementioned problem. As shown in Figure 1, we can use the variational approach, based on the Pontryagin's Maximum Principle. However, this approach could not handle properly with inequality constraints (in our case, we deal with such constraints since the velocities are bounded). Other strategies applying an NLP solver can be used. This involves replacing the time-dependent variables by discretised ones, such as coefficients of an interpolation polynomial, for example, so that an NLP problem can be formulated and solved with respect to these new discretised variables. The first strategy is the sequential approach: in this case, only the control variables are discretised. For a set of control variables, a DAE solver in a loop solves the state variables of the DAE system and returns the state and algebraic variables to the NLP optimisation level. The control variables (in fact the discretised variables that represent them) are updated by the NLP solver. This strategy can be time-consuming. In the second strategy, the simultaneous approach, both state and control variables are discretised in time. Hence, the DAE system is solved only once, at the optimal point, and therefore this can avoid computational effort to obtain intermediate solutions for the DAE system.

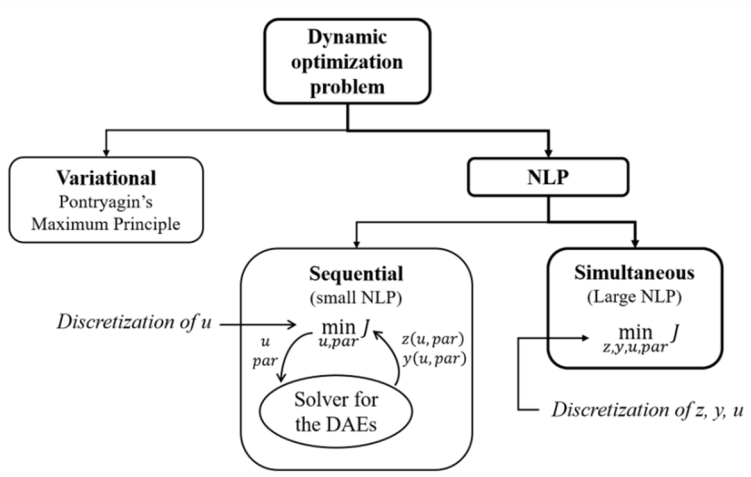

Figure 1. Solution strategies for dynamic optimisation

Many authors have suggested using Orthogonal Collocation on Finite Elements (OCFE) to discretise the state and/or control variables when DAEs are constraints of the dynamic optimisation problem [20-22] (or [23-25]).

With this in mind, in the present study, we use a simultaneous approach using 2D-OCFE. The equation that describes the transient temperature profiles in the pipes is a partial differential equation. Variables are then discretised in time and space.

In order to contribute to the field of dynamic optimisation of district cooling system (DCS) operation, we propose a methodology that enables a simultaneous (oriented-equation) solution of this dynamic optimisation problem using 2D Orthogonal Collocation on Finite Elements (2D-OCFE). We apply this methodology to a medium-sized cooling system serving 20 consumers of different categories with fluctuating cooling demands, subject to variable external conditions. The dynamic simulation and optimisation were performed using insulated and non-insulated piping.

First, the configuration of the studied cooling network is described, including the consumers' demand profile and the external conditions to which it is subject. Next, we present the resulting problem, then the proposed discretisation strategy, which consists in transforming the Partial Differential Algebraic Equation (PDAE) problem into a purely algebraic problem, by implementing 2D Orthogonal Collocation on Finite Elements (2D-OCFE) for the dynamic simulation (DS) of the case study. Based on this formulation, we structure the operational objective function for the optimisation problem. Finally, we discuss the results of the simulation and optimisation problems. This work is the first stage of a project that aims to develop a methodology for the optimal management of a cooling network, considering the dynamics of the whole system, including conversion, storage, and energy distribution.

2 Cooling system

We develop a dynamic analysis of an academic case study, with conditions based on real data. The system consists of 20 users distributed over an urban area in known locations. Based on this distribution, we propose a set of nodes and pipes that connect the production site and the users. Next, we build the cooling demand profile for each user based on typical performances for various kinds of building, as reported by an industrial supplier of cooling services. Finally, we present the external conditions to which the system will be subject.

2.1 Configuration of the system

The topology of the system is based on the illustrative example presented by Söderman [13]. From the coordinates the author presented for the location of the users, it is possible to compute the lengths of the pipes, as detailed in Table 2.

Table 2. Lengths of main and lateral pipes of the system

Main pipes			Lateral pipes		
Pipe		Length (m)	Pipe		Length (m)
0	0_r	50	in_{C_1}	out_{C_1}	40
1	1_r	279.93	in_{C_2}	out_{C_2}	0.1
2	2_r	720.07	in_{C_3}	out_{C_3}	242.99
3	3_r	176.46	in_{C_4}	out_{C_4}	95.21
4	4_r	124.69	in_{C_5}	out_{C_5}	110.64
5	5_r	397.32	in_{C_6}	out_{C_6}	227.56
6	6_r	124.97	in_{C_7}	out_{C_7}	102.58
7	7_r	338.27	in_{C_8}	out_{C_8}	0.43
8	8_r	198.19	in_{C_9}	out_{C_9}	147.38
9	9_r	478.17	$in_{C_{10}}$	$out_{C_{10}}$	330.51
10	10_r	147.01	$in_{C_{11}}$	$out_{C_{11}}$	110.62
11	11_r	73.54	$in_{C_{12}}$	$out_{C_{12}}$	154.73
12	12_r	279.38	$in_{C_{13}}$	$out_{C_{13}}$	0.32
13	13_r	382.3	$in_{C_{14}}$	$out_{C_{14}}$	404.71
14	14_r	190.01	$in_{C_{15}}$	$out_{C_{15}}$	95.14
15	15_r	12.13	$in_{C_{16}}$	$out_{C_{16}}$	371.66
16	16_r	268.79	$in_{C_{17}}$	$out_{C_{17}}$	363.38
17	17_r	1280.6	$in_{C_{18}}$	$out_{C_{18}}$	371.94
18	18_r	198.28	$in_{C_{19}}$	$out_{C_{19}}$	91.03
19	19_r	32.89	$in_{C_{20}}$	$out_{C_{20}}$	0.1
20	20_r	438.04			

Using this information, Figure 2 presents a scheme of the cold network, main pipes (0-20), lateral pipes $(in_{C_1} - in_{C_{20}})$, the nodes and the users, in a simplified way that is useful for modelling purposes. As shown in Table 2, the complete system also includes a return network, represented by the return pipes (0_r - 20_r and $out_{C_1} - out_{C_{20}}$) with the same lengths as the outward path pipes. Thus, the whole network is an arrangement of 82 pipes with a total length of almost 19 km (18904.11 m).

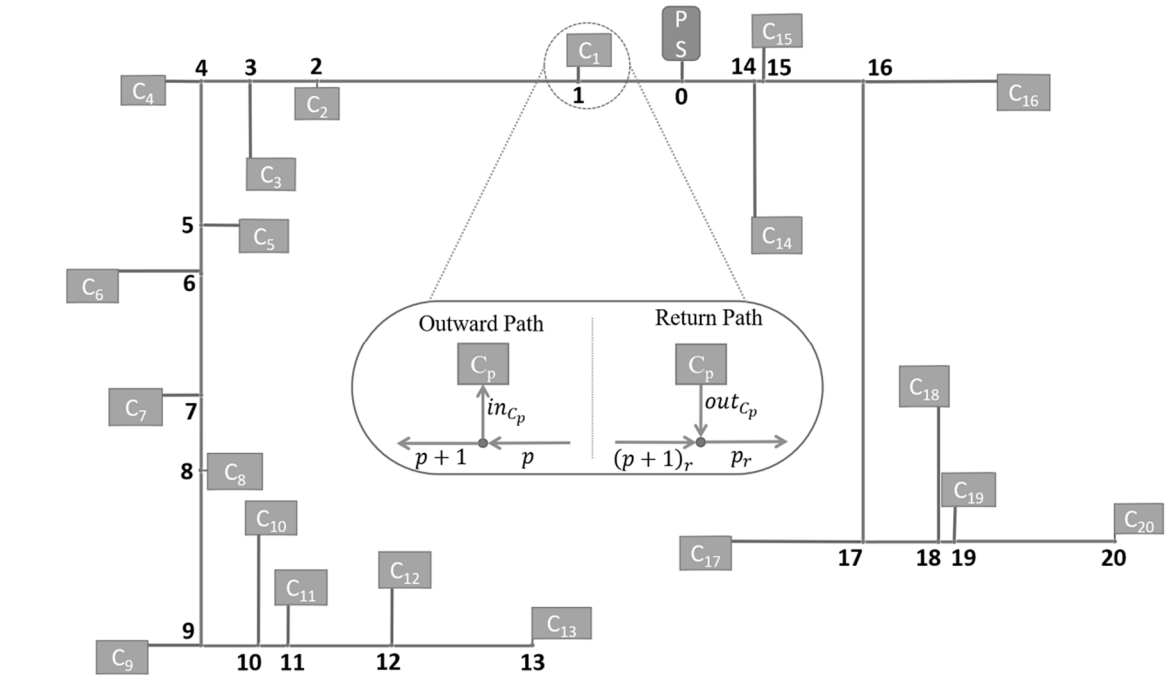

Figure 2. Representation of the cooling network

To define the diameters of the pipes, we take into account the recommended flow velocities for sizing cooling water pipes, as reported by Branan [26] and presented in Table 3. The system must respect the velocity bounds during the simulation and optimisation analysis.

Table 3. Maximum allowable speeds in pipes

Pipe size (in)	Maximum velocity (ms^{-1})	
	in mains pipes	in laterals pipes
2	--	1.31
3	0.94	1.32
4	1.08	1.54
6	1.29	1.69
8	1.27	1.76
10	1.37	1.86
12	1.56	2.08
14	1.56	2.19
16	1.80	2.41
18	1.90	2.53

Pipe size (in)	Maximum velocity (ms^{-1})	
	in mains pipes	in laterals pipes
20	2.03	--

2.2 Users' demand profiles

For this work, we built cooling demand profiles based on the daily cooling demand curves presented by Olama [27] for different kinds of buildings including office, residential, hotel or service, apartments, shopping and leisure. These profiles represent the variation in demand with respect to the peak cooling load of the buildings, as seen in Figure 3.

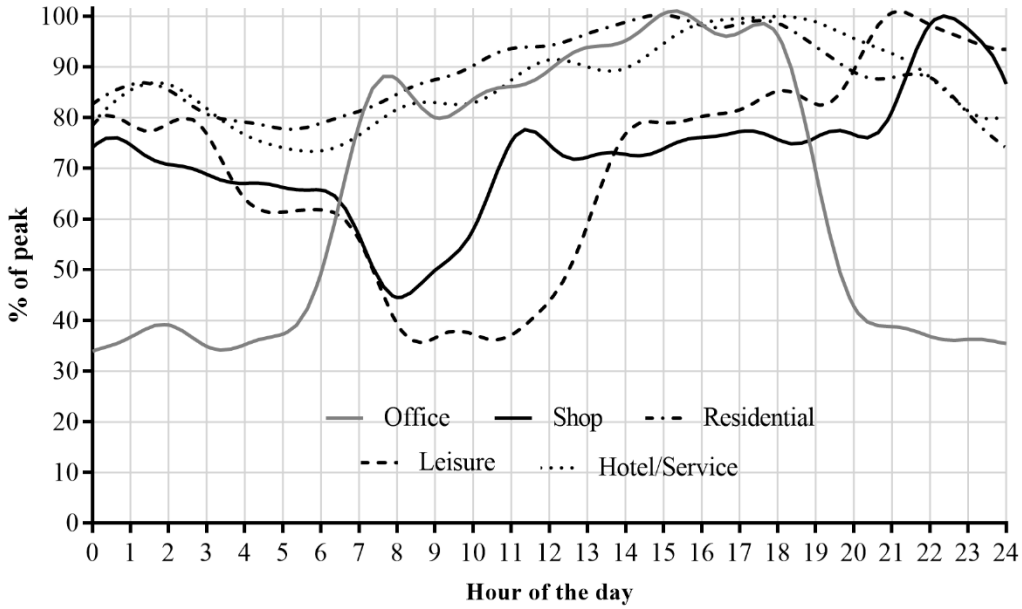

Figure 3. Demand for different kinds of building

Using the peak cooling demands presented by Söderman for this system [13], which are based on real data (Table 4), and the aforementioned profiles we can compute the demand profiles of the 20 consumers.

Table 4. Peak demands for users in the Network

Consumer	Type	Maximum load (kW)	Consumer	Type	Maximum load (kW)
C_1	Shop	1640	C_{11}	Residential	800
C_2	Office	700	C_{12}	Office	100
C_3	Leisure	200	C_{13}	Shop	180
C_4	Office	780	C_{14}	Office	1500
C_5	Shop	100	C_{15}	Hotel/Services	650
C_6	Office	900	C_{16}	Hotel/Services	380
C_7	Office	100	C_{17}	Leisure	455
C_8	Residential	250	C_{18}	Hotel/Services	900
C_9	Hotel/Services	400	C_{19}	Leisure	360

Consumer	Type	Maximum load (kW)	Consumer	Type	Maximum load (kW)
C_{10}	Office	170	C_{20}	Leisure	1220

Considering these data, Figure 4 presents the total cooling demand profile of the district cooling system and details the specific demand of two consumers (for the sake of clarity). The maximum demand of the network is 10911 kW and is reported at 17.64 h (t_{max}). We will use the demand of each consumer reported at this time $Q_{Cp}(t_{max})$ for dynamic simulation analysis.

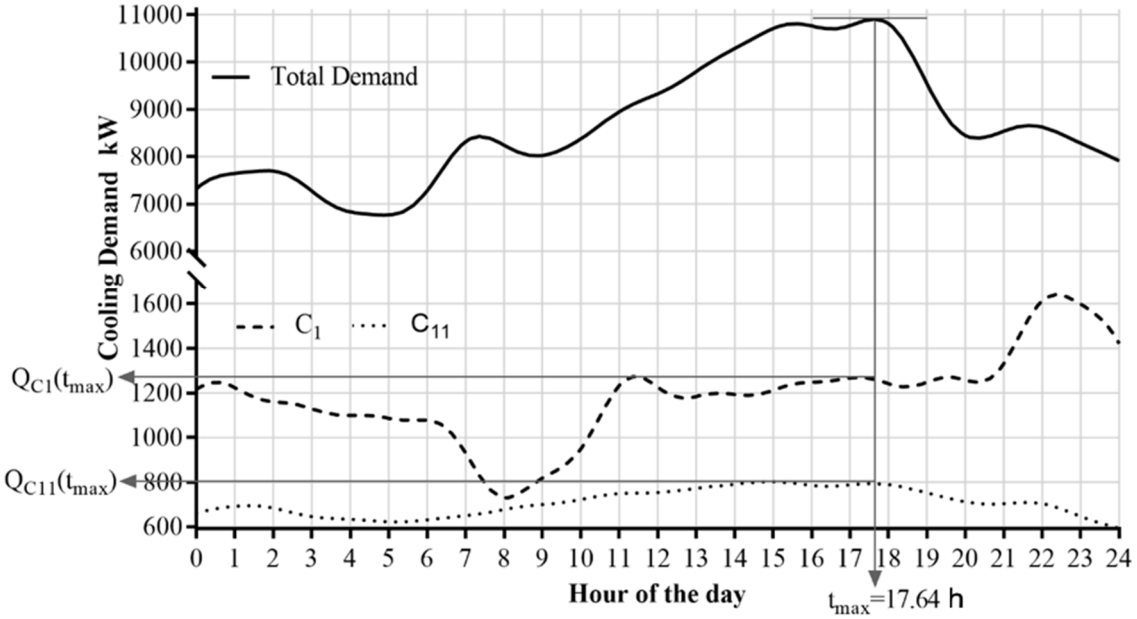

Figure 4. Total and some specific cooling demands of the system

We will study the system under different external conditions, including various kinds and characteristics of soil as well as differentiated ambient temperatures corresponding to different climate zones.

2.3 Studied climate zones

The kind of soil and its moisture affect its thermal conductivity, as reported in the ASHRAE district cooling guide [28].

Table 5. Soil thermal conductivities

Soil Moisture (By mass)		Thermal conductivity ($Wm^{-1}K^{-1}$)		
		Sand	Silt	Clay
Low	<4%	0.29	0.14	0.14
Medium	4%-20%	1.87	1.30	1
High	>20%	2.16	2.16	2.16

In order to analyse the implementation of a district cooling network in different climate areas and its impact on the total thermal resistance and on the thermal distribution in the pipes, we chose three cases (cities) with different daily ambient temperature profiles and soil characteristics, as detailed below:

- Ras Al Khaimah (UAE): Low moisture; sandy soil.
- Paris: Medium moisture; clay soil
- Kuala Lumpur (KL): High moisture; clay soil

Figure 5 details the profile temperature on the hottest day in 2018 for each of the selected cities. These profiles were built using real data from the Weather Underground global community, which collects data from more than 250,000 weather stations around the world [29].

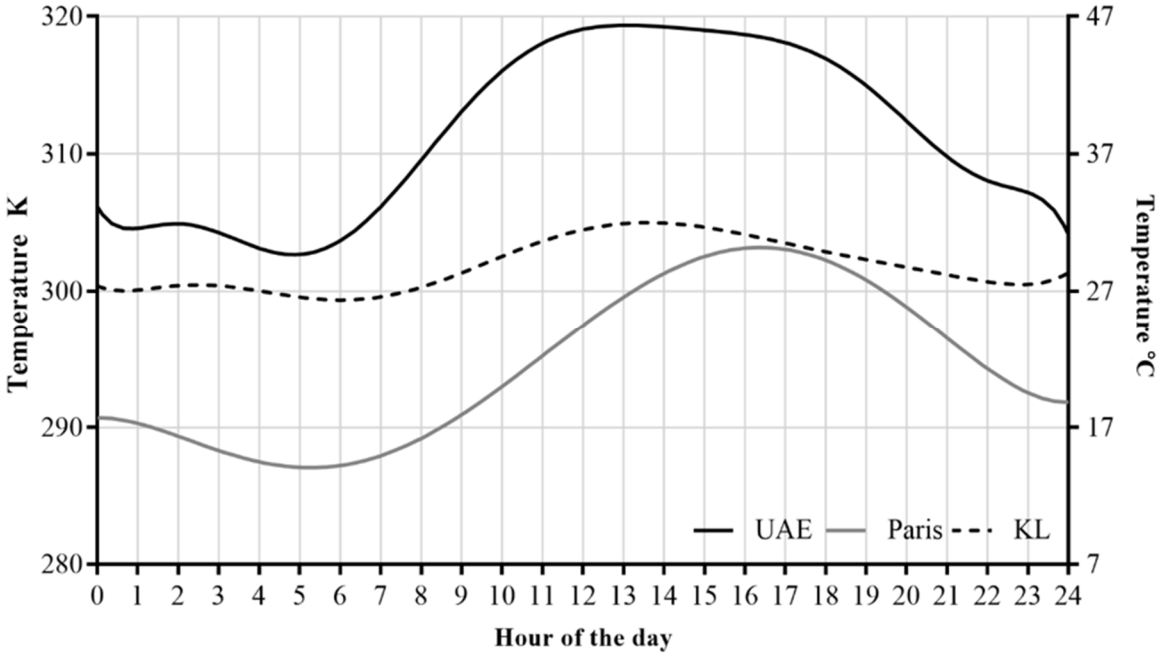

Figure 5. Summer temperature profiles in the studied climate zones

With the system configuration already defined, we can complete the mathematical model that describes the dynamic operation of the network and develop a proper strategy for its solution.

3 Mathematical model

The model of the DCS is constituted by the heat transfer equation in each pipe, together with mass and energy balances at each node of the system, under the following assumptions:

- The system uses water as cooling fluid (w).

- The mass flow in each pipe is time-dependent and uniform.
- The physical properties of the fluid are constant.

3.1 Heat balance in the pipes

Most of the available literature on dynamic modelling and optimisation of district energy systems focus their interest in the analysis of district heating systems. Nevertheless, these models can also be applied to district cooling [30]. Studies on equation-based methods for the analysis of energy networks [17,31,32] use a dynamic one-dimensional heat transfer equation to describe the temperature transients in the pipes, defined as:

$$\rho_w \cdot Cp_w \cdot A \cdot \frac{\partial T(t,x)}{\partial t} + \dot{m}(t) \cdot Cp_w \cdot \frac{\partial T(t,x)}{\partial x} = \frac{T_s - T(t,x)}{R'} \quad (6)$$

where ρ_w, Cp_w, A, and $\dot{m}$ are the density, specific heat capacity, area (cross-section), and mass flow rate of water in the pipe, respectively; R' is the total thermal resistance per unit length of pipe; T stands for temperature in the pipe, T_s for the temperature of the soil surface, and t and x for time and distance dependency.

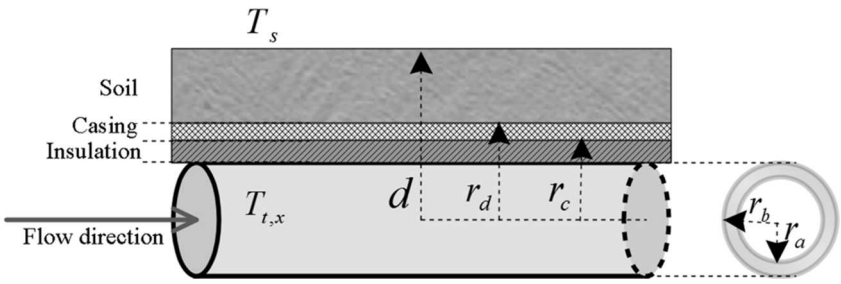

Figure 6. Representation of a buried pipe

This heat equation is subject to the following assumptions:

- ✓ Plug flow
- ✓ Heat transfer is considered only in the radial direction
- ✓ Conduction heat transfer is considered through the pipe, the insulation, the casing and the soil
- ✓ Material properties are constant and independent of temperature.
- ✓ It does not include thermal interactions between supply and return pipes
- ✓ Thermal inertia of the pipes, the casing and the insulation is neglected
- ✓ Conductive heat transfer in the fluid is neglected

The total thermal resistance per unit length of pipe, R', is a function of the thermal conductivities of the pipe, λ_{ab}, the insulation, λ_{bc}, the casing, λ_{cd}, and the soil, λ_s, as follows [31]:

$$R' = \frac{1}{2\pi r_a \bar{h}} + \frac{ln\left(\frac{r_b}{r_a}\right)}{2\pi\lambda_{ab}} + \frac{ln\left(\frac{r_c}{r_b}\right)}{2\pi\lambda_{bc}} + \frac{ln\left(\frac{r_d}{r_c}\right)}{2\pi\lambda_{cd}} + \frac{1}{S\lambda_s} \quad (7)$$

Expressions to compute the conduction shape factor S are detailed in Chapter 4 of reference [33], and the average convection heat transfer coefficient in the pipe $\bar{h}$ can be computed as:

$$\bar{h} = \frac{\overline{Nu}\lambda_w}{2r_a} \quad (8)$$

where we can use the Dittus-Boelter equation [34] to compute the average Nusselt number $\overline{Nu}$.

The solution of equation (6) has been addressed using mainly discretisation (partial or total) or 1D analytical solutions coupled with physical approximations. Discretisation strategies include the implementation of finite volumes [35], finite elements [36], and finite differences [37]. On the other hand, estimates are based on a succession of steady states, as proposed by Duquette *et al*. [31], or the Lagrangian approach of Zhou *et al*. [38]. In this second group, we can also include the contributions of Stevanovic *et al*. [39], van der Heijde *et al*. [32] and Schweiger *et al*. [17]. These last two contributions use an implementation in Modelica®, where the fluid and temperature propagations are calculated separately from the heat loss, combining a plug flow approach with an ideal mixed volume model. These methods require a large number of grid points for discretisation, or a large storage memory to compute the behaviour of the temperature in the pipes for the steady-state-based methods. It could be pointed out here, that several of these studies ([31, 32, 38]) have validated the previous model, based on reasonable assumptions, by comparison with experimental data.

However, for some dynamic modelling applications in chemical engineering [40,41], the orthogonal collocation method has been used to handle Partial Differential Equation (PDE) problems. If applied to the space domain, the orthogonal collocation method transforms a PDE system into an Ordinary Differential Equation (ODE) system (where time is the only integration variable) which is smaller in size than that obtained using a classical discretisation strategy (e.g. Finite differences). The resulting ODE system can be solved using classical methods, like Runge-Kutta (RK) as carried out by Ebrahimzadeh *et al*. [41], who reported computational times up to 90% lower compared to the Method of Lines (i.e. finite differences in space and RK in time).

When the nature of the phenomenon demands more accurate measurements, the domain of integration can be divided into subdomains or finite elements, where the orthogonal collocation method is implemented, allowing the use of a large number of grid points. Biegler [42] reported better convergence and lower computational requirements for the OCFE method compared to other discretisation methods.

To describe the dynamics of the district system, we must couple the 82 Partial Differential Equations (PDE) (6) (one for each pipe) with the mass and energy balances in the connections between the network and the users, represented by linear and nonlinear algebraic equations presented in the next section. This leads to a Partial Differential Algebraic Problem (PDAE), which is solved in the present work using 2D-OCFE, transforming the PDAE system into a set of algebraic equations. Thus, we can solve the dynamic optimisation of the DCS using a simultaneous strategy.

3.2 Heat balances in the nodes

Initial condition

For each pipe k, the initial spatial temperature profile is known from a steady-state simulation:

$$T_k(0,x) = \theta_k(x) \tag{9}$$

Here, $\theta_k(x)$ represents the spatial distribution of temperature along pipe k at $t = 0$. The way to achieve this steady-state simulation will be discussed later.

Boundary conditions

We assume that chilled water is produced at a constant temperature (277 K). For the pipe leaving the production site ($p = 0$), we then have:

$$T_0(t,0) = 277\ \text{K} \tag{10}$$

The nodes in the outward path are splitters, where the outlet temperature of the pipe entering the node is equivalent to the inlet temperature of the pipe leaving it:

$$\begin{gathered} T_{p-1}\left(t, L_{p-1}\right) = T_p(t,0) \quad , p = 1 \dots 13{,}15, \dots 20 \\ T_0(t, L_0) = T_{14}(t,0) \\ T_p\left(t, L_p\right) = T_{in_{C_p}}(t,0) \quad , \quad p = 1 \dots 20 \end{gathered} \tag{11}$$

where L_k is the length of pipe k. k may be $p, p_r, in_{C_p}, out_{C_p}$.

On the other hand, heat balances for the return path and the consumers ($C_p = (C_1, C_2, \dots, C_{20})$) will define the boundary condition of the pipes leaving these elements of the system. As we consider constant properties, they will be:

$$\dot{m}_{p_r}(t)\cdot T_{p_r}(t,0)=\dot{m}_{(p+1)_r}(t)\cdot T_{(p+1)_r}\left(t,L_{(p+1)_r}\right)+\dot{m}_{out_{C_p}}(t)\cdot T_{out_{C_p}}\left(t,L_{out_{C_p}}\right),$$

$$p=1\ldots12{,}14,\ldots19$$

$$\dot{m}_{0_r}(t)\cdot T_{0_r}(t,0)=\dot{m}_{1_r}(t)\cdot T_{1_r}\left(t,L_{1_r}\right)+\dot{m}_{14_r}(t)\cdot T_{14_r}\left(t,L_{14_r}\right) \quad (12)$$

$$\dot{m}_{p_r}(t)\cdot T_{p_r}(t,0)=\dot{m}_{out_{C_p}}(t)\cdot T_{out_{C_p}}\left(t,L_{out_{C_p}}\right)\ ,\ p=13\,,20$$

$$Q_{C_p}(t)=\dot{m}_{in_{C_p}}(t)\cdot \mathrm{C}p_w\cdot\left(T_{out_{C_p}}(t,0)-T_{in_{C_p}}\left(t,L_{in_{C_p}}\right)\right) \quad (13)$$

where $T_{in_{C_p}}\left(t,L_p\right)$ and $T_{out_{C_p}}(t,0)$ are the inlet and outlet temperatures of the exchanger.

3.3 Mass Balances in the nodes

For the nodes and consumers, the mass balances are given by:

Outward path

$$\dot{m}_p(t)=\dot{m}_{p+1}(t)+\dot{m}_{in_{C_p}}(t)\quad p=1\ldots12{,}14\ldots19$$

$$\dot{m}_p(t)=\dot{m}_{in_{C_p}}(t)\quad p=13\,,20 \quad (14)$$

$$\dot{m}_0(t)=\dot{m}_1(t)+\ \dot{m}_{14}(t)$$

Return path

$$\dot{m}_{p_r}(t)=\dot{m}_{(p+1)_r}(t)+\dot{m}_{out_{C_p}}(t)\quad p=1\ldots12{,}14\ldots19$$

$$\dot{m}_{p_r}(t)=\dot{m}_{out_{C_p}}(t)\quad p=13\,,20 \quad (15)$$

$$\dot{m}_{0_r}(t)=\dot{m}_{1_r}+\ \dot{m}_{14_r}$$

Consumers

$$\dot{m}_{in_{C_p}}(t)=\dot{m}_{out_{C_p}}(t)\ \ p=1\ldots20 \quad (16)$$

With the heat and energy balances of the system already formulated, the next section presents the analysis of degrees of freedom of the system and the supplementary relationships that we included in order to have zero degrees of freedom for simulation purposes.

3.4 Degrees of freedom and flow policy

From the set of equations (6) and (9) to (16), the degrees of freedom of the system can be analysed for the 82 pipes at each instant t, as detailed in Table 6. The number of degrees of freedom of the

system is 20 at each instant t, representing the profiles to be given for dynamic simulation or computed via dynamic optimisation.

Table 6. Analysis of degrees of freedom of the system

Variables		Equations		
Variable	# of variables	Equation	# of equations	
$T_k(x,t)$	82	(6)	**82**	
		1st order in t and x PDE requires per pipe:		
		- **1** Initial Condition (9)	82	
		- 1 Boundary Condition (10)	1	
		(11)	40	82
		(12)	21	
		(13)	20	
$\dot{m}_k(t)$	82	(14)	21	
		(15)	21	**62**
		(16)	20	

Considering this, for dynamic simulation purposes we must complete the degrees of freedom of the system. We can do this by defining the flow policy we will use to achieve the cooling demand for each consumer. Some systems operate under constant production conditions, as shown in Figure 7, where the production of cold ($\dot{m}_0$) and the mass flow in the main network ($\dot{m}_p$ and $\dot{m}_{in_{C_p}}$) are constant at the level necessary to cover the peak of the total demand of the system. In this way, the producer guarantees enough cold in the system during the studied period, but this results in cost overruns for production and pumping of the chilled water. At each consumer substation, there is a common pipe $Cm(t)$ connecting the main and return networks, to regulate the flow to the consumer ($vin_{C_p}(t)$) over time, sending large quantities of cold water directly to the return network in periods of low demand, and the total flow of $\dot{m}_{in_{C_p}}$ to the consumers when their demand corresponds to the peak. The literature reports this policy as constant-primary secondary-variable flow [27,28].

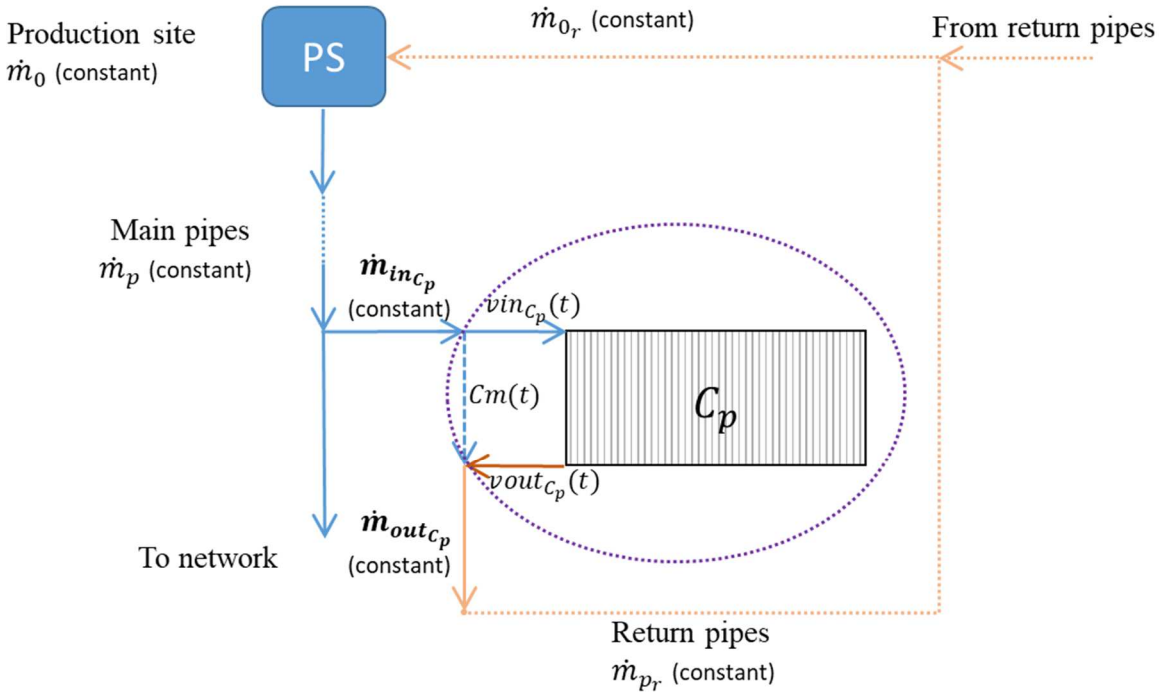

Figure 7. Constant flow policy diagram

To represent constant flow in the main network, we first define a constant mass flow leaving the production site by:

$$\dot{m}_0(t) = \dot{m}_{0\mathrm{Cte}} \tag{17}$$

Furthermore, in the splitters, we assume that the mass flows entering the consumers at each time ($\dot{m}_{in_{C_p}}(t)$) are proportional to their corresponding maximum peak demand ($Peak(C_p)$ from Table 4). We can do this by fixing the ratio between these variables for all the consumers over time as:

$$\frac{Peak(C_1)}{\dot{m}_{in_{C_1}}} = \frac{Peak(C_p)}{\dot{m}_{in_{C_p}}}, \quad \forall\, p \in \{2, \dots, 20\} \tag{18}$$

The mass and energy balances presented in section 3.3 are the balances for each consumer for the boundaries defined by the dotted borderline presented in Figure 7. Hence only the mass flows $\dot{m}_{in_{C_p}}$ are computed; the pipes $Cm(t)$, $vin_{C_p}(t)$ and $vout_{C_p}(t)$ belong to the user's substation and their flows are not considered in this analysis.

The dynamic response of the system will initially be analysed under constant production mass flow $\dot{m}_{0\mathrm{Cte}}$ as expressed in (17). This value corresponds to the value of the producer mass flow in steady-state, which is computed using relations (18) and imposing a return temperature (19) to complete the 20 degrees of freedom.

$$T_{0_r}(L_{0_r}) = 287 \text{ K} \tag{19}$$

Then, to simulate the constant flow policy in the dynamic simulation, the 20 degrees of freedom at each time t are completed using (17) and (18).

The optimisation analyses include the study of the constant flow policy and optimisation of the system operation using a dynamic flow policy. In the former case, (17) and (18) will be constraints and the value $m_{0\text{Cte}}$ will be the only optimisation variable. In the latter case, these constraints are not considered, giving the profiles $\dot{m}_0(t)$ and $\dot{m}_{inC_p}(t), p = 1 \dots 20$ as optimisation variables.

Finally, as mentioned in section 2.1, the flow velocity $v_{k,e,i}$ inside a pipe k, cannot exceed its maximum allowed velocity $v_{max,k}$ reported in Table 3.

$$v_{k,e,i} \leq v_{max,k} \tag{20}$$

With this inequality, we complete the mathematical model that we will use to describe the dynamics of the proposed district cooling distribution system.

4 Formulation of the optimisation problem

With the mathematical model already defined, this section describes the operational optimisation applications of the DCS. We present the operational objective function, which will be analysed for different degrees of freedom. Lastly, we detail the methodology used to obtain the initialisation and the solution of the resulting NLP problem.

For the present application, we will use a Lagrange problem type formulation, which will measure the influence of the variations in cold demands $Q_{C_P}(t)$ and of the soil surface temperature $T_s(t)$ on the systems, with the aim is to achieve a given operational condition over the studied time horizon.

In our case, the control variables are the mass flow in each pipe $\dot{m}_k(t)$. They are called control variables because they are the variables which will have to be manipulated to manage the system online. It should be noted, however, that the dynamic optimisation we do here is not an online control: it consists in the offline calculation of the temporal profiles of these control variables. The known soil temperature $T_s(t)$ as well as the demand of each consumer $Q_{C_P}(t)$ are treated as algebraic variables, which are not optimisation variables. The velocities $v_k(t)$ are optimised algebraic variables. The lengths of the pipes L_k are time-independent parameters. In our case, the differential state variables are the temperature in each pipe, T_k, which depend not only on t but also on x. Instead of dealing with

DAE constraints, we then deal with PDAE constraints. It can be noted that applying a space discretisation method to the temperatures leads to DAE constraints, while increasing the number of "state variables" dependent only on t (variable $T_k(t,x)$ is replaced by nl variables $T_{kl}(t)$).

4.1 Objective function

The efficiency of a DCS is measured in terms of the difference between the temperature of the fluid leaving the production site and the temperature of the fluid that returns to it (ΔT). Generally, maintaining a high ΔT reduces the flow rates of the chilled water system and the costs of the distribution system due to the use of smaller pipe diameters. This results in savings in pumping energy costs and improves operating costs [27]. Typically, ΔT in the DCS production site is maintained at around 8-12°C [28,43].

When the ΔT is not properly controlled, the DCS could present an important issue known as "*low ΔT syndrome*" [27]. Indeed, this low ΔT at the production site is a consequence of a low ΔT at each consumer, which is a symptom of the low efficiency at the consumer's substation. Then, in order to satisfy the consumers' demands, the system has to pump excess rates of chilled water although the plant is not designed to operate at this level. A high ΔT design is generally economical to the operation of a district cooling station, the chilled water distribution network, and individual buildings' heating, ventilating and air conditioning (HVAC) systems. This is because of savings in the size of piping and accessories in the plant and larger savings in piping, pre-insulation, and accessories in the chilled water distribution network.

To optimize ΔT and meet customer demand, both the flow from the central plant and flow on the customer's side must be varied [28]. These variations also represent savings in pumping energy. The complete dynamic flow policy of the system is represented in Figure 8. This operating policy eliminates the use of the common pipe shown in the case of the constant flow policy (Figure 7) and the resulting mixing and possible reduction in the temperature in the return network.

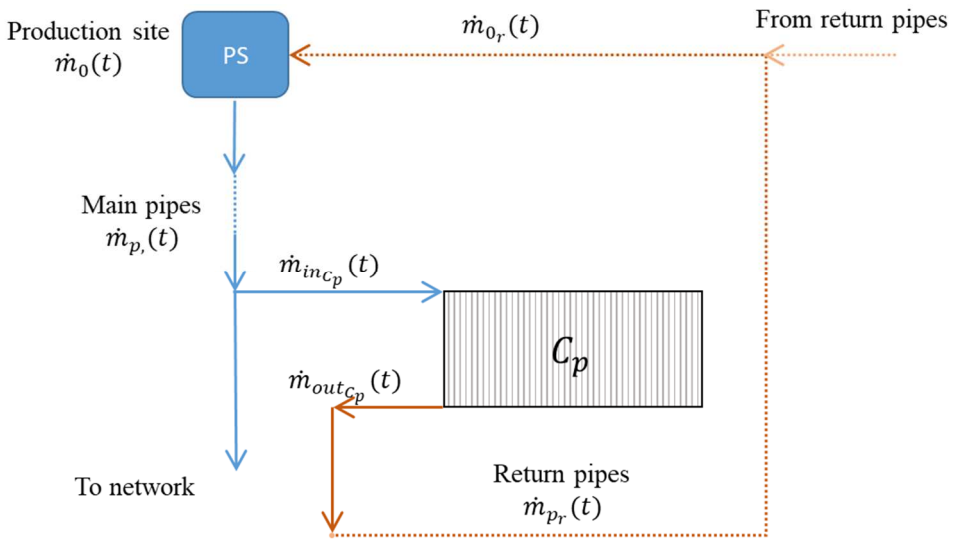

Figure 8. Dynamic flow policy diagram

The variations in temperature mentioned above represent not only a technical issue but also an economic impact on the customer. The consumer will be charged 3% for each degree Celsius of the monthly average return temperature below the system design return temperature [27]. On the other hand, it is important to avoid high temperatures that might compromise the proper operation of the production site technology.

Bearing this in mind, we define J as the quadratic error between the outlet temperature of the users and a set point. First, we analyse the system under the constant flow policy (21), and then we perform the optimisation for a dynamic operation (22), for a design outlet temperature of 287K.

$$\min_{\substack{\dot{m}_{0Cte} \\ Var}} \sum_{p} \left(\int_0^{24} \left(T_{outC_p}(t) - 287 \right)^2 dt \right)$$
$$S.t.\,(6),(9)\ to\ (16),(17),(18),(20) \tag{21}$$

Since a constant flow policy is applied, equation (17) is embedded in the set of model equations. We also apply the flow policy equation (18), which requires that the ratios of the splitters are constant. In this optimisation, therefore, the only control variable is the constant flow leaving the producer $\dot{m}_{0Cte}$. Var represents all the other variables of the problem $(T(t,x), \dot{m}_k(,t), \ldots)$ whose optimal paths minimise the difference between the consumers' outlet temperature and the proposed design temperature over time. The flow variables $\dot{m}_k(t)$ are treated as algebraic variables.

$$\min_{\substack{\dot{m}_{in_{C_p}}(t) \\ var}} \sum_{p} \left(\int_0^{24} \left(T_{outC_p}(t) - 287 \right)^2 dt \right)$$
$$S.t.\ (6),\quad (9)\ to\ (16),(20) \tag{22}$$

In this case, none of the constant flow policy equations (17) and (18) are included in the model, so that the mass flow of the producer and the ratios of the splitters are time-dependent and will be the main control variables.

4.2 Discretisation strategy

As stated in section 1 in the present work, we use 2D-OCFE to transform equation (6) into a set of algebraic equations, which is highly advantageous and efficient for simultaneous optimisation applications[21]. To our knowledge, there are no studies related to the dynamic operation of DCSs that use OCFE to handle the resulting PDAE problem.

The generalities of the numerical method and its implementation in discretising equation (6) are presented in Appendix A. Based on this implementation, we present the discretised mathematical model of the system in Appendix B. nf elements containing $nj + 1$ collocation points are used to discretise the space domain and ne elements containing $ni + 1$ collocation points are used to discretise the time domain. The choice of the value of these parameters is discussed in section 5. Finally, in order to verify the accuracy and the validity of the results obtained with this kind of discretisation, comparisons with other classical methods are proposed in Appendix C.

4.3 Methodology for the solution of the dynamic simulation and optimisation problems

A good initial guess for the optimisation of dynamic systems is crucial for a fast and reliable solution to a dynamic optimization problem, as stated by Safdarnejad *et al*. [44]. Figure 9 describes the procedure we implemented to obtain the initial guess and solve the PDAE problem.

Due to the lack of piping data for the selected system [13], we define the diameters using an iterative procedure, which uses the maximum allowable speed flows as decision criteria. For this purpose, we first compute a theoretical maximum mass flow in the main pipe using a model without heat losses that includes only the heat and mass balances in the nodes and consumers, for the maximum demand (peak demand) of each consumer and a return temperature of 287 K (which is also the outlet temperature of each consumer exchanger since heat losses are neglected). We then evaluate the maximum speed constraints consecutively, looking for the smallest diameter of each pipe that could transport the computed flow without exceeding the allowable speeds. It is important to mention that the diameters chosen for this iterative step will lead us to a physically achievable operation, but they are not optimal regarding any economic or operational criteria. The computation of the optimal diameter of the pipes is beyond the scope of the present work.

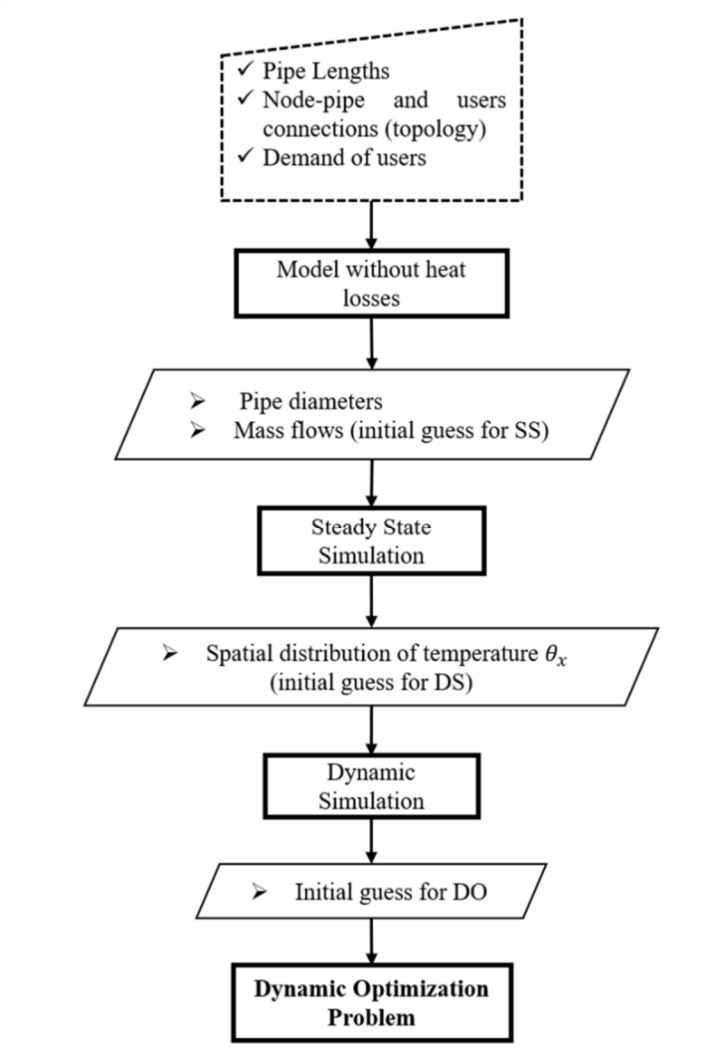

Figure 9. Schematic representation of the solution strategy

With the diameters already defined, we run the model without heat losses for the maximum demand of the system (demand in $t = 17.64\ h = t_{max}$, presented in Figure 4), and the result represents the initialisation to solve the steady-state (SS) problem. This problem is defined by the equation system (6), (9) to (18) and (20), with $\frac{\partial T}{dt} = 0$, external conditions in $t = 0$ and user demand fixed to its value at $t = t_{max}$. The main result of this problem is the spatial distribution of temperature $\theta_k(x)$ for each pipe k for the constant flow policy, which represents the initial condition for the dynamic problem and the initial guess for its solution. This distribution is given by the temperature values at the spatial collocation points $\theta_{k,f,j}$. With this, it is possible to solve the fully dynamic simulation (DS) problem (Equations (6), (9) to (18) and (20)), that describes the behaviour of the complete system, subject to the environmental and operational perturbations over the selected time horizon. Finally, we use the solution of the DS as the initial guess for the dynamic optimization (DO) problem. We implement all the described stages in the GAMS modelling environment and solve the

562 different problems using the CONOPT feasible path solver, on a 2.7 GHz quad-core CPU with 8 Gb of
563 RAM.
564

565 # 5 Results and discussion

566 We present the results according to the flowchart presented in Figure 9. First, we analyse the
567 computed pipe diameters of the cooling network pipes using the model without heat losses. These
568 diameters become inlet data (parameters) for the forthcoming problems. The second result is the
569 distribution of temperatures computed by the steady-state simulation for the system under the external
570 conditions described in section 2.3. Lastly, we present dynamic analyses (DS and DO) of the case with
571 major variations in the steady-state simulations.

572 ## 5.1 Pipe diameters

573 Using the abovementioned iterative procedure with the model without heat losses, we define the
574 distribution of pipe diameters detailed in Table 7.
575
576 **Table 7. Pipe diameters for the DCS**

Pipe size (in)	Pipes	# of pipes
20	0, 0_r	2
16	1, 1_r	2
14	2, 2_r, 14, 14_r	2
12	3, 3_r, 4, 4_r, 5, 5_r, 6, 6_r, 15, 15_r, 16, 16_r, 17, 17_r	16
10	7, 7_r, 8, 8_r, 18, 18_r	6
8	9, 9_r, 10, 10_r, 11, 11_r, 19, 19_r, 20, 20_r, in/outC_1, in/outC_{14}	14
6	in/outC_2, in/outC_4, in/outC_6, in/outC_{11}, in/outC_{15}, in/outC_{18}, in/outC_{20}	14
4	12, 12_r, in/outC_9, in/outC_{16}, in/outC_{17}, in/outC_{19}	10
3	13, 13_r, in/outC_3, in/outC_8, in/outC_{10}, in/outC_{13}	10
2	in/outC_5, in/outC_7, in/outC_{12}	6
Total		82

577

578 These diameters ensure the operation of the system under the proposed demand profiles and they
579 will be fixed parameters for the subsequent problems.
580

581 Under these conditions, the producer pumps a total flow of 259.66 kg s^{-1} of chilled water, to supply
582 the cooling demand corresponding to the maximum demand of the network (t_{max}). The distribution of
583 diameters presented here is consistent because the sizes of the pipes decrease the further away they are
584 from the production site. Furthermore, the smallest pipes feed those users with lower cooling
585 demands. With these data, we define the global thermal resistance per unit length R' of the pipes. To
586 compute the thermal resistances, we assume that all the pipes are buried at the same depth of one

meter (d in Figure 6). The thermal conductivities and thickness of the insulation correspond to the values reported by the North American Insulation Manufacturers Association [45].

Figure 10 shows the variation in the global thermal resistance with respect to the pipe diameters for insulated and non-insulated pipes, for the characteristic terrain and initial soil temperature for each of the proposed climate zones detailed in section 2.3. These values will also be input parameters for the forthcoming problems.

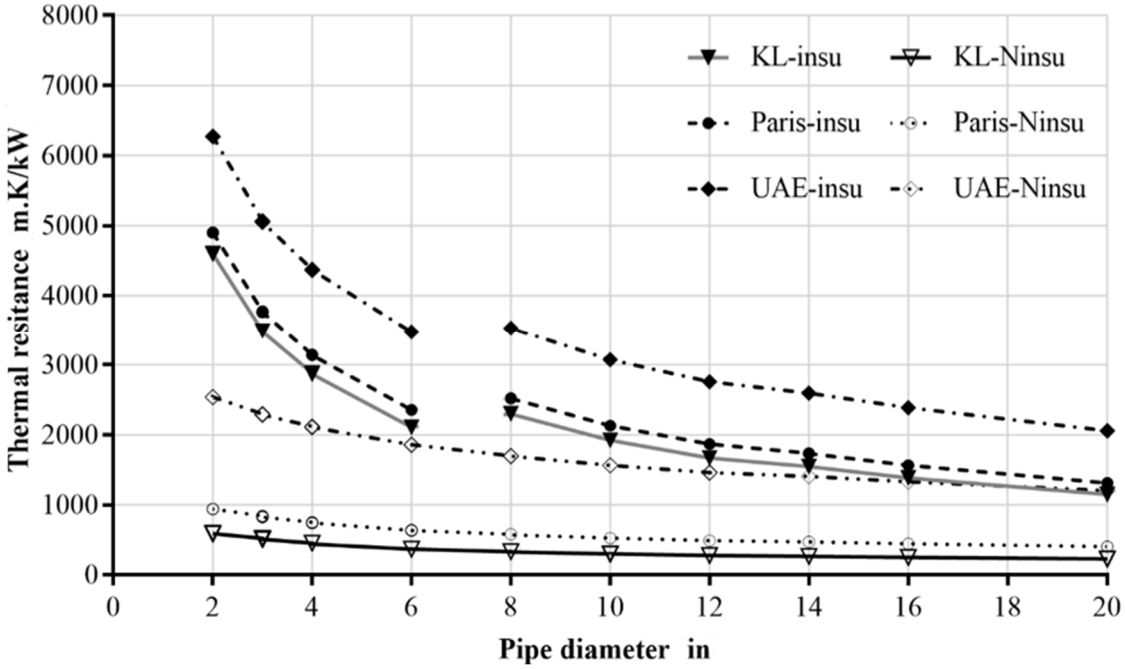

Figure 10. Variation in total thermal resistance

We can show that in all cases, as the pipe diameter increases, the value of the global thermal resistance decreases, resulting in a major variation for insulated pipes. For both kinds of pipe, installation under KL conditions has a lower thermal resistance. The discontinuity of *R'* for the insulated pipes corresponds to a change in the insulation thickness, which is one inch for pipes with diameters smaller than 8 inches and 1.5 inches for the others. Furthermore, for large insulated pipes (16" and 20") the resistance in KL is equivalent to that computed for non-insulated pipes under UAE conditions. These values will have a major influence on the spatial distributions of temperature, as we will discuss in the next subsection.

5.2 Steady-state simulations

With all the elements of the distribution network already established, it is necessary to define the number of elements (nf) and points ($nj + 1$) that will be used to solve the DS and DO problems. To do this, we perform several simulations, changing the number of elements ($nf = 1,2,3,5$) and points inside each element ($nj + 1 = 4,6,11$) (e.g. the degree of the Lagrange interpolation polynomial is =

3,5,10), and compare the results. We chose the combination of elements and points with the lowest CPU time where the solution did not present significant variations compared with the solution obtained with the maximum number of points. Using this procedure, we chose $nf = 1$ and $nj + 1 = 11$. Later, using the same procedure for dynamic simulations, we define $ne = 24$ and $ni + 1 = 6$.

We completed the steady-state simulation for the climate (using $T_s\,(t = 0)$ as external temperature) and soil conditions presented in section 2.3 using insulated and non-insulated pipes. For each climate zone, the simulation was first performed for a system with insulated pipes, fixing the return temperature $\theta_{0_r,nf,nj}$ to compute the producer mass flow $\dot{m}_{0Cte}$. This latter is set as a parameter for the system with non-insulated pipes, where we compute the return temperature in order to compare the influence of the insulation under the same flow conditions. Table 8 details these results.

Table 8. Results for steady-state simulations

	Insulated pipes			**Non-insulated pipes**		
	KL	Paris	UAE	KL	Paris	UAE
$\dot{m}_{0Cte}\ (kg\ s^{-1})$	263.6	261.4	262.9	263.6	261.4	262.9
$\theta_{0_r,nf,nj}\ (K)$	287	287	287	287.7	287.2	287.1

As expected, the system that reported the lowest thermal resistance (KL) demands more cold water from the provider to achieve the proposed return temperature using insulated pipes. On the other hand, although the UAE presents the biggest thermal resistance, this location also represents the hottest external temperatures, resulting in a bigger mass flow compared with the network installed in Paris. Moving to the systems with non-insulated pipes, the variation in the return temperature increases as the thermal resistance decreases. Although the non-insulated system in UAE presents a slightly smaller variation than that in Paris, the producer must pump more cold water, resulting ultimately in a greater operational cost.

Figure 11 details the spatial distribution of temperature over the left outward branch of the network (C_1 to C_{13} in Figure 2; the production site is located at $x = 0$). The solution of the steady-state model for each climate condition takes less than 0.5 s.

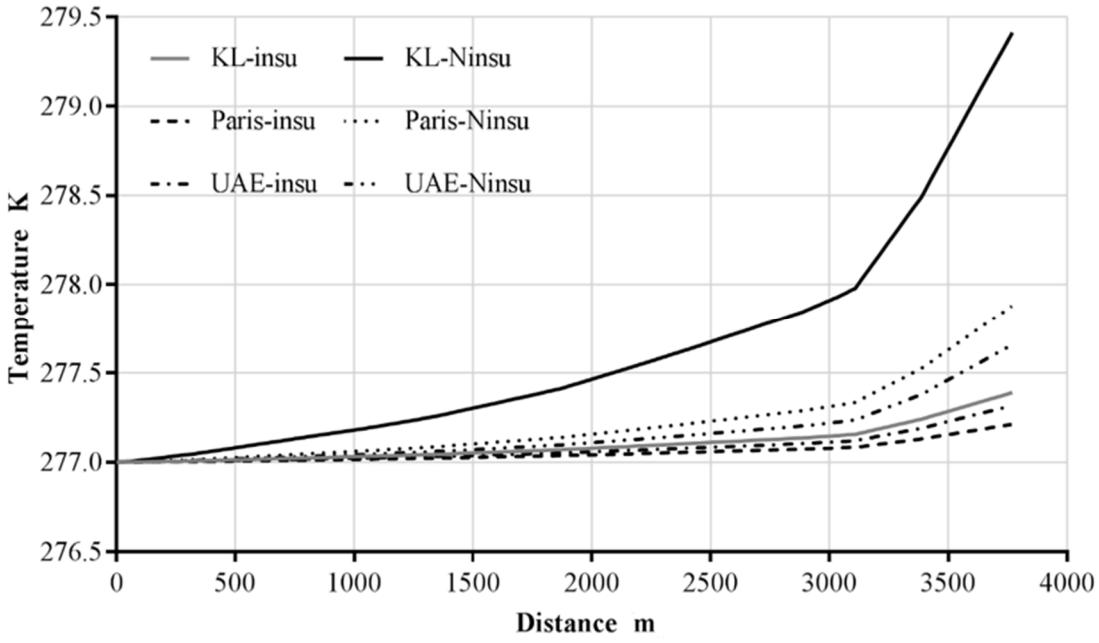

Figure 11. Spatial distribution of temperature in the outward path for the left side of the network

We observe in all cases that the water in the pipes increases in temperature as it moves further from the production site. As expected, results under the humid conditions in Kuala Lumpur present the biggest temperature increments. Although the variations in spatial temperature are of the order of 0.5 K or less, its computation will have a large impact on the dynamic study of the system under variable flows. Furthermore, the computed mass flows aim to cover the maximum demand of the system.

These results agree with the total pipe resistances presented in Figure 10. The system with the lowest thermal resistance values has the greatest spatial temperature variations. In the light of these results, the dynamic analysis of the system will be performed for the external conditions in KL.

5.3 Dynamic simulation

As stated in equation (17), the producer mass flow is fixed at its computed steady-state value (Table 8) for the dynamic simulations. Figure 12 details the temperature profile at the outlet of consumers 1 and 11, for both insulated and non-insulated pipes. We chose these consumers because of their high demand and to show the impact of the distance from the producer site. The CPU times reported for solving the dynamic simulation problem were 56.7 s for the system with insulated pipes and 46.8 s for the network without insulation.

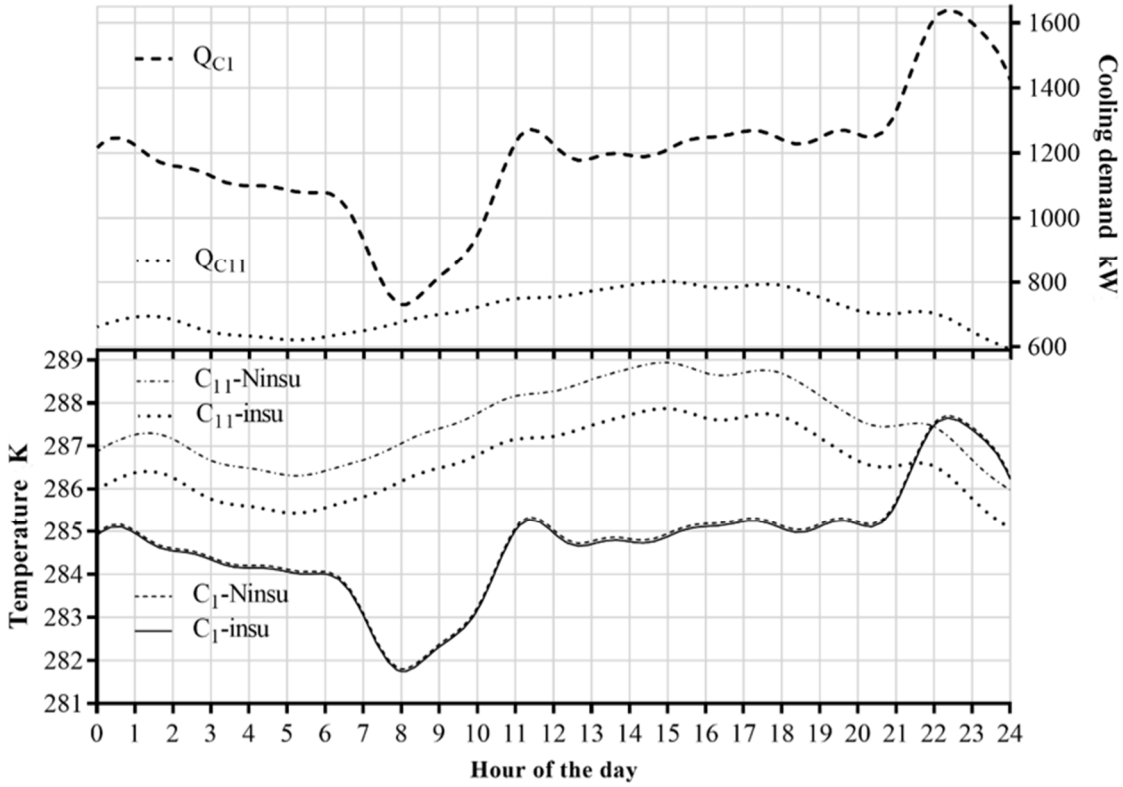

Figure 12. Outlet temperature in consumers 1 and 11 for constant flow policy under KL conditions

Using the constant flow policy, the consumers' outlet temperature will vary over time in line with the corresponding demand. This results in a non-uniform return temperature to the production site, as shown in Figure 13. For both insulated and non-insulated pipes, the return temperature ($T_{0_r}(t, L_{0_r})$) is influenced by the total demand profile. These profiles exhibit a lag time compared to the profile of the total demand. This lag time represents the interval of time it takes for the fluid leaving each user to arrive at the production site. These variations in return temperature represent a technical issue at the production site due to the need for production at the cold utility to stay close to the design temperature [46]. Furthermore, the operation under this flow policy drives the system to the undesired low ΔT syndrome, with ΔT values at the production site as low as 6.28K.

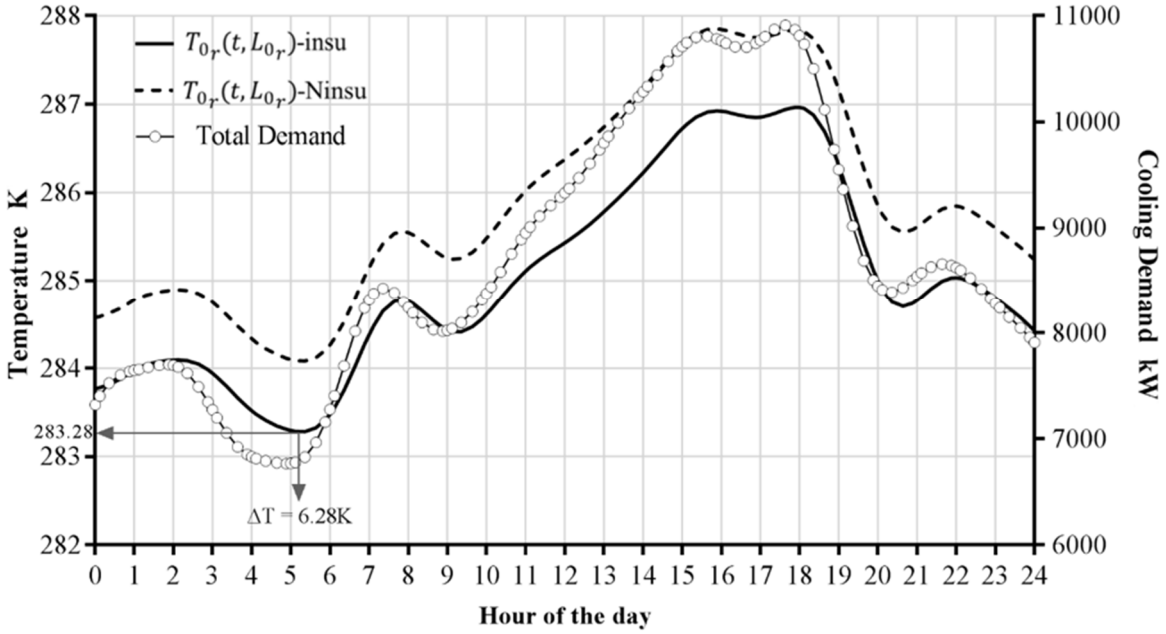

669
670 **Figure 13. Return temperature under constant flow policy for KL conditions**
671

672 As stated in section 4.3, the solution described for the dynamic simulation problem will be used as
673 the initial guess for the optimisation problems, whose results are detailed in the next section.

674 ## 5.4 Dynamic optimisation

675 The DO problem stated in the formulation (21) aims to evaluate the potential of the constant flow
676 policy to maintain the system under the desired conditions of operation. For this problem, the only
677 control variable is the constant flow at the production site. Figure 14 presents the temperature profiles
678 of the return and outlet pipes of the chosen consumers for both insulated and non-insulated pipes. In
679 terms of CPU time, the solution of problem (21) required 70 s and 58 s for insulated and non-insulated
680 pipes respectively.
681

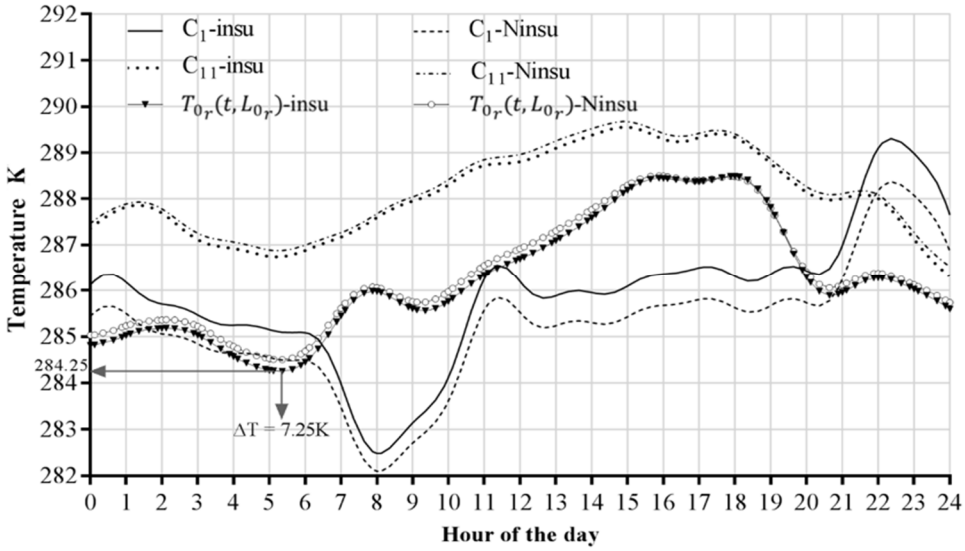

Figure 14. Optimisation of the constant flow operation

For insulated pipes, the optimal producer mass flow is 228.36 kg s^{-1}, while for the non-insulated system it is 248.40 kg s^{-1}, which represents an increment of 8.7% in the quantity of chilled water produced for the non-insulated system. Although the system presents a higher ΔT (7.25 K) compared with the simulation results, the return temperature still presents variations, which would compromise the operation of the central cooling plant [46].

As expected, for consumer C_{11} the outlet temperature is higher when using non-insulated pipes. On the other hand, under the same conditions, consumer C_1 presents a lower outlet temperature. This is due to the influence of distance on the inlet temperature of each consumer, and the larger mass flows for the non-insulated systems. Figure 15 details the inlet temperature profiles for consumers C_1 and C_{11}, located at 370 m and 3219 m from the producer, respectively.

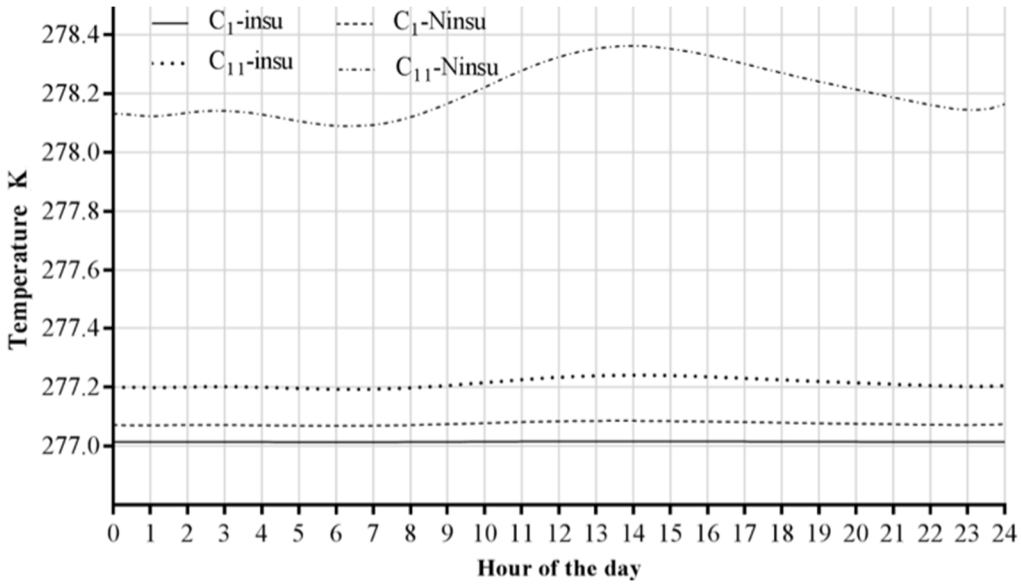

Figure 15. Inlet Temperature profile for selected consumers under constant flow

We can show the influence of distance from the source when we use non-insulated pipes. The difference in the values of the outlet temperature for C_1 when the kind of pipe is changed ranges from 0.05 K to 0.06 K, while for C_{11} this difference ranges from 0.89 K to 1.2 K. C_1 is, therefore, operating at almost the same temperature in both cases, but due to the increment of the inlet mass flow to the consumer (31.77 kg s^{-1} to 34.57 kg s^{-1}), the outlet temperature is lower when using non-insulated pipes. This phenomenon was also observed in consumers C_2, C_3, C_4 (1446 m from production site), C_{14}, C_{15} and C_{16} (892 m from production site).

The previous results show that when working with the constant flow policy, it is not possible to operate the system under the desired parameters. Although the return temperature is warmer, its variation due to the demand profiles of the consumers prevents proper operation of the cooling network.

By implementing a dynamic flow policy, on the other hand, as stated in the optimisation problem in (22), the system will operate with more uniform return temperatures, using insulated and non-insulated pipes, as detailed in Figure 16.

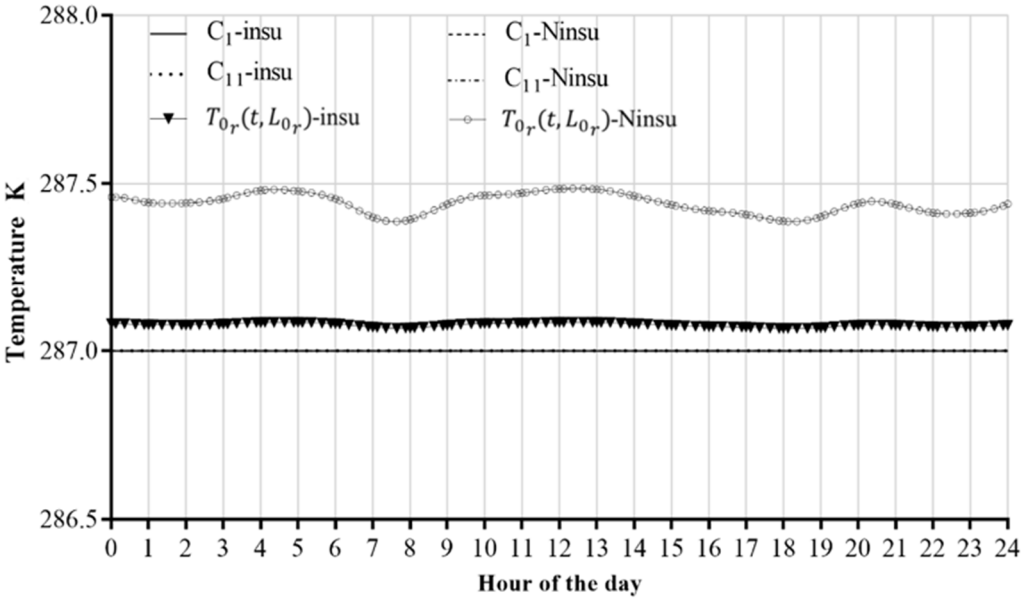

Figure 16. Temperature profiles for dynamic flow policy

Solving this problem took 517 s and 334 s for insulated and non-insulated pipes respectively. It is important to note that this problem has a total of 2520 degrees of freedom, which corresponds to the value of the 20 inlet mass flows and production in the 120 collocation points in time.

As expected, the return pipe in the insulated network presents a lower temperature than the non-insulated one. Nevertheless, the only way to achieve the desired outlet temperature in the non-

insulated pipe for all consumers involved exceeding the maximum allowed speed in the pipes, as shown in Table 9. Although the velocity violations are small (the largest is 0.24 ms^{-1} for pipes 13 and 13_r) they should involve changing the corresponding pipes to implement a system without insulation. However, for the sake of simplicity and to avoid having to recalculate previous simulations, we did not change the diameters, but we increased the maximum velocity slightly. Contrary to Branan [26], the American Society of Heating, Refrigerating and Air-Conditioning Engineers (ASHRAE) [47,48] does not report a maximum allowable velocity depending on pipe size and indicates that in any case (irrespective of application, size or material) the velocity in the pipes cannot exceed 4.6 ms^{-1}. As detailed in Table 9, none of the pipes reports values even close to 2m/s. Although in these cases the velocity bounds have been violated, the computed solution leads to reliable system operation. This shows the lack of precision when using an approximation without heat losses to define the diameters of the pipes, and the advantage of including the pipe diameter as an optimisation variable in future studies.

Table 9. Pipes exceeding allowed velocities in non-insulated network

pipes	**v (ms^{-1})**	**maximum velocity (ms^{-1})**	**pipes**	**v (ms^{-1})**	**maximum velocity (ms^{-1})**
$9/9_r$	1.37	1.27	in/out8	1.42	1.32
$13/13_r$	1.18	0.94	in/out12	1.36	1.31
$19/19_r$	1.28	1.27	in/out20	1.72	1.69

Figure 17 presents the optimal inlet mass flows for the selected consumers and for the production site. The computed mass flows consider the heat gains required along the pipes to meet the fluctuating consumer demand, reducing the variation in the outlet temperature for each consumer and hence, the uncontrolled deviation in the return temperature.

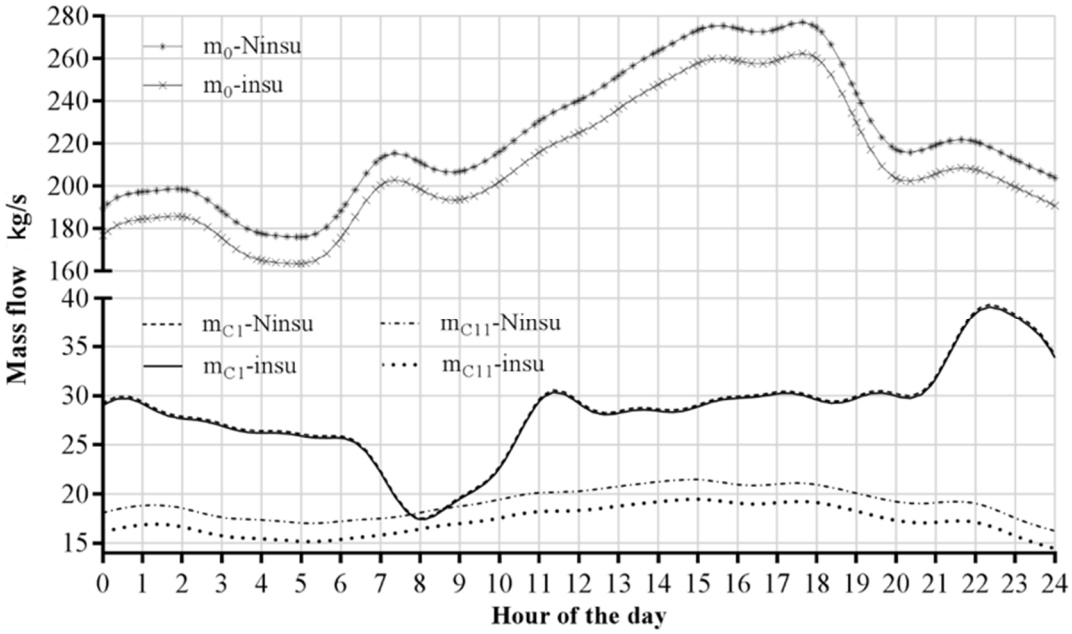

Figure 17. Optimal production and inlet mass flow for chosen consumers

As expected, the non-insulated system requires more cold water. However, due to the heat gains and the kind of demand, this difference is not proportional among all the users, as can be seen when comparing the profiles of C_{11} (3219 m from production site) and C_1 (370 m from production site).

Finally, it is possible to compute the total production required per day using the pumping methodologies presented here for the two kinds of piping as $\int_0^{24} \dot{m}_0(t)dt$. We present these results in Table 10, where DO.1 and DO.2 refer to the solution of problems (21) and (22) respectively.

Table 10. Total chilled water production for the studied pumping methods

Total production Ton				
DS	DO.1-insu	DO.1-Ninsu	DO.2-insu	DO.2-Ninsu
22775.13	19730.68	21462.09	18141.78	19329.01

The optimal dynamic policy (DO.2) represents a reduction of 8.06% (insulated) and 9.94% (non-insulated) compared with the computed productions using a constant flow (DO.1). Compared with the production using the constant flow policy in dynamic simulation, the reductions are 20.34% and 15.42% respectively. The system operates at the desired levels of temperature only if a complete dynamic policy is used.

6 Conclusions

In this contribution, we presented an innovative solution methodology, based on 2D-OCFE, for the dynamic simulation and dynamic optimisation with a non-restrictive computational time of district cooling systems. The chosen model was based on reasonable assumptions and was already validated with experimental data in other studies [31, 32, 38]. Using this method, it was possible to fully

discretise the initial differential problem, transforming the differential operators into algebraic combinations of the state variable at some collocation points in time and space. This results in a simultaneous solution of the optimisation problem, which involved solving steady-state and dynamic simulations to properly initialise it. Using this methodology, we analyse a medium-sized cooling network, including environmental and demand variations over a time horizon of 24 h.

The proposed strategy allowed solving the discretised model (that accounted with more than 360000 variables) with CPU times around 50 s for dynamic simulation and less than 600 s for dynamic optimization. Via dynamic simulation, we computed the operational response of the system when a constant flow policy is implemented, resulting in undesirable levels of temperature of the water returning to the production site leading to a low ΔT in the production site (as low as 6.28 K). Considering this, we proposed an objective function to control the temperature of the water leaving the clients implementing a dynamic flow policy to avoid the reported low ΔT syndrome.

We computed the optimal paths for mass flow at the production site and the consumer substations to optimise the operation of the network using insulated and non-insulated pipes. Optimisation allowed to synchronize the energy production with the total demand of the system resulting in a lower production of chilled water to supply the consumer's demand for the two kinds of piping (20.34% and 15.42% respectively) compared with the production computed via dynamic simulation.

The results of the optimisation presented here show the capability of the proposed methodology to improve the operating conditions of DCSs under varying cooling demands and external conditions. It might be interesting to make a comparison with experimental data in order to consolidate our methodology or to validate some numerical values used in the model (i.e. thermal conductivity of the soil, convective heat transfer coefficient…). Given the reported CPU times, this method represents a suitable starting point for a more complex analysis of DCSs, including optimal simultaneous operation and design.

We are currently working on the techno-economic analysis of the system, aiming to include the diameter of the pipes as optimisation variables and to compute properly the electrical requirement to pump the chilled water to the consumers. In future work, we intend to study the network when chilled water storage technology is included and to develop the MIDO model in order to choose the most appropriate technology for producing chilled water.

Appendix A. Generalities and implementation of OCFE

A collocation method approximates the unknown solution (the state variable) of an ordinary differential equation as a finite sum of known trial functions and enforces the ordinary differential equation to be satisfied at some collocation points. If the trial functions are Lagrange basis polynomials, if the integration variable is normalised, and the collocation points are chosen as roots of orthogonal polynomials, then the method is called orthogonal collocation. When using the OCFE method, the state variable is approximated by a different interpolating polynomial on each finite element, and the state variable continuity must be ensured at the boundaries.

A.1. One-dimensional case:

Let us consider an example where the spatial variable is the only integration variable (1D case), it can be the model of our DCS in steady-state conditions. If the whole domain is divided into nf elements (x_{f-1} and x_f being the boundaries of the fth element and L_f its length) and if the state variable is approximated by a polynomial of order nj (e.g. $nj+1$ collocation points are used on each element), then the state variable (e.g. temperature) can be expressed on the fth element as the following Lagrange interpolation polynomial:

$$T(\xi) = \sum_{j=0}^{nj} T_{f,j}\, \ell_j(\xi) \tag{A-1}$$

with:

$$\xi = \frac{x - x_{f-1}}{x_f - x_{f-1}} = \frac{x - x_{f-1}}{L_f} \quad , \xi \epsilon [0,1] \tag{A-2}$$

the normalised spatial variable, and

$$\ell_j(\xi) = \prod_{\substack{k=0 \\ k \neq j}}^{nj} \frac{\xi - \xi_k}{\xi_j - \xi_k} \tag{A-3}$$

the jth Lagrange basis polynomial of degree nj.

With such trial functions (e.g. Lagrange basis polynomial), the coefficient of the jth trial function on the fth element represents the variable at the collocation point ξ_j (i.e. $T(\xi_j) = T_{f,j}$).

Then the implementation of the collocation method consists in writing that the differential equation is satisfied on each collocation point ξ_j. In each element f: the state variable is replaced by $T_{f,j}$, the derivative can be calculated by deriving the Lagrange interpolation polynomial, leading to a linear combination of the $nj+1$ coefficients $T_{f,k}$ $(k=0,\dots nj)$. Then the differential equation satisfied at this collocation point ξ_j finally leads to an algebraic equation involving the $nj+1$ coefficients $T_{f,k}$ $(k=0,\dots nj)$. Finally, by solving the system of all these $nf\times(nj+1)$ algebraic equations we obtain the $nf\times(nj+1)$ values $T_{f,j}$ of the temperature at these collocation points.

In order to estimate the derivative terms, Hedengren *et al.* [22] have proposed a convenient method, which includes the boundary condition. We have adapted it to collocation on finite elements and describe it below. It begins with a classical formulation of the Lagrange interpolation polynomial on the f[th] element (equation (A-4)):

$$T(\xi)=\alpha_0+\alpha_1\xi+\alpha_2\xi^2+\alpha_3\xi^3+\cdots+\alpha_{nj}\xi^{nj} \tag{A-4}$$

The first step is then to find a matrix M_x that relates the values of the derivative at the collocation points and the coefficients as follows:

$$\begin{bmatrix}\frac{dT}{d\xi}(\xi_1)\\ \frac{dT}{d\xi}(\xi_2)\\ \vdots\\ \frac{dT}{d\xi}(\xi_{nj})\end{bmatrix}=M_x\left(\begin{bmatrix}T_{f,1}\\ T_{f,2}\\ \vdots\\ T_{f,nj}\end{bmatrix}-\begin{bmatrix}T_{f,0}\\ T_{f,0}\\ \vdots\\ T_{f,0}\end{bmatrix}\right) \tag{A-5}$$

The coefficient α_0 corresponds to the boundary condition of the element f, $T_{f,0}$, when the initial position is defined as zero. For the first element, this value ($T_{1,0}$) must be given, whereas for the following elements it corresponds to the final value of the previous element. Then, substituting the approximation of the state variable and its derivative in the previous expression $T_{f,0}$ will be cancelled and it follows:

$$\begin{bmatrix}1 & 2\xi_1 & 3\xi_1^2 & \cdots & nj\xi_1^{nj-1}\\ 1 & 2\xi_2 & 3\xi_2^2 & \cdots & nj\xi_2^{nj-1}\\ & & \vdots & & \\ 1 & 2\xi_{nj} & 3\xi_{nj}^2 & \cdots & nj\xi_{nj}^{nj-1}\end{bmatrix}\begin{bmatrix}\alpha_1\\ \alpha_2\\ \vdots\\ \alpha_{nj}\end{bmatrix}=M_x\begin{bmatrix}\xi_1 & \xi_1^2 & \cdots & \xi_1^{nj}\\ \xi_2 & \xi_2^2 & \cdots & \xi_2^{nj}\\ & & \vdots & \\ \xi_{nj} & \xi_{nj}^2 & \cdots & \xi_{nj}^{nj}\end{bmatrix}\begin{bmatrix}\alpha_1\\ \alpha_2\\ \vdots\\ \alpha_{nj}\end{bmatrix} \tag{A-6}$$

Finally, considering the change of variable, this leads to:

$$\begin{bmatrix} \left(\frac{dT}{dx}\right)_{f,1} \\ \left(\frac{dT}{dx}\right)_{f,2} \\ \vdots \\ \left(\frac{dT}{dx}\right)_{f,nj} \end{bmatrix} = \frac{1}{L_f} \cdot M_x \left(\begin{bmatrix} T_{f,1} \\ T_{f,2} \\ \vdots \\ T_{f,nj} \end{bmatrix} - \begin{bmatrix} T_{f,0} \\ T_{f,0} \\ \vdots \\ T_{f,0} \end{bmatrix} \right) \tag{A-7}$$

$$= \frac{1}{L_f} \cdot \begin{bmatrix} 1 & 2\xi_1 & 3\xi_1^2 & \cdots & nj\xi_1^{nj-1} \\ 1 & 2\xi_2 & 3\xi_2^2 & \cdots & nj\xi_2^{nj-1} \\ & & \vdots & & \\ 1 & 2\xi_{nj} & 3\xi_{nj}^2 & \cdots & nj\xi_{nj}^{nj-1} \end{bmatrix} \begin{bmatrix} \xi_1 & \xi_1^2 & \cdots & \xi_1^{nj} \\ \xi_2 & \xi_2^2 & \cdots & \xi_2^{nj} \\ & & \vdots & \\ \xi_{nj} & \xi_{nj}^2 & \cdots & \xi_{nj}^{nj} \end{bmatrix}^{-1} \left(\begin{bmatrix} T_{f,1} \\ T_{f,2} \\ \vdots \\ T_{f,nj} \end{bmatrix} - \begin{bmatrix} T_{f,0} \\ T_{f,0} \\ \vdots \\ T_{f,0} \end{bmatrix} \right)$$

Once the collocation points are defined, we can calculate the collocation matrix M_x and discretise the derivative terms using equation (A-7) to obtain a set of algebraic equations whose resolution will give the solution to the differential problem. For the present application, we use the nodes of the shifted Legendre Gauss Lobatto quadrature as collocation points [49]. Thus, 0 and 1 are nodes and there are $nj - 1$ internal nodes. It follows that:

$$T_{f,0} = T_{f-1,nj} \qquad f = 2, \dots nf \tag{A-8}$$

Then, on each element, the ODE has to be written only on nj points (ξ_j, $j = 1 \dots nj$) since the boundary condition (e.g. $T_{f,0} = T\left(L_f \xi_0 + x_{f-1}\right) = T\left(x_{f-1}\right)$) of each element is known. When dealing with a steady-state simulation, the above methodology has been applied to our DCS and the temperature, which depends only on x, has been noted $T(t\ fixed, x) = \theta(x)$.

In the following subsection, we present the implementation of the method for both time (t) and space domains (x).

A.2. Implementation of 2D-OCFE

The orthogonal collocation on finite elements method in 2 dimensions can be formulated as an extension of the 1D derivation, as stated by Surjanhata[50], Finlayson[40] and Esche *et al.*[23], using the corresponding variables for each direction as well as a different polynomial or number of roots. First, the time horizon is divided into ne intervals (finite elements), and inside each interval, ni collocation points are chosen. Similarly, each pipe has nf segments with nj collocation points. Therefore, we define sets $e \in (1,2, \dots, ne), i \in (0,1, \dots, ni), f \in (1,2, \dots, nf), j \in (0,1, \dots, nj)$. We also introduce the normalised time for element e (similarly to the normalised spatial variable):

$$\tau = \frac{t - t_{e-1}}{t_e - t_{e-1}} = \frac{t - t_{e-1}}{\Delta t_e} \quad , \tau \epsilon [0,1] \tag{A-9}$$

Let us then consider the temperature of the spatial-time domain corresponding to element e in time and element f in space. This is now approximated by the following function of ξ and τ (degree ni in τ and nj in ξ):

$$T(\tau, \xi) = \sum_{i=0}^{ni} \sum_{j=0}^{nj} T_{e,i,f,j}\, \ell_i(\tau) \ell_j(\xi) \tag{A-10}$$

The properties of the Lagrange basis polynomials lead to $T(\tau_i, \xi_j) = T_{e,i,f,j}$ and therefore:

$$T(\tau, \xi_j) = \sum_{i=0}^{ni} T_{e,i,f,j}\, \ell_i(\tau) \tag{A-11}$$

and:

$$T(\tau_i, \xi) = \sum_{j=0}^{nj} T_{e,i,f,j}\, \ell_j(\xi) \tag{A-12}$$

To compute $\frac{\partial T}{\partial \tau}(\tau_i, \xi_j)$ we will derive the Lagrange interpolation polynomial described by equation (A-11). This represents the evolution in time of the temperature in the present element (e) for the given position (f, j) and involves coefficients $T_{e,l,f,j}$ with e, f, j fixed, and l varying from 0 to ni (and passing through the particular value i), which are represented by ⧅ in Figure A-1. The same logic applies to compute $\frac{\partial T}{\partial \xi}(\tau_i, \xi_j)$: we will derive the Lagrange interpolation polynomial described by equation (A-12) which represents the evolution in space of the temperature in the present element (f) for the given time (e, i). It involves the coefficients $T_{e,i,f,l}$ with e, i, f fixed, and l varying from 0 to nj (passing through the particular point j), and represented by ⧄ in Figure A-1.

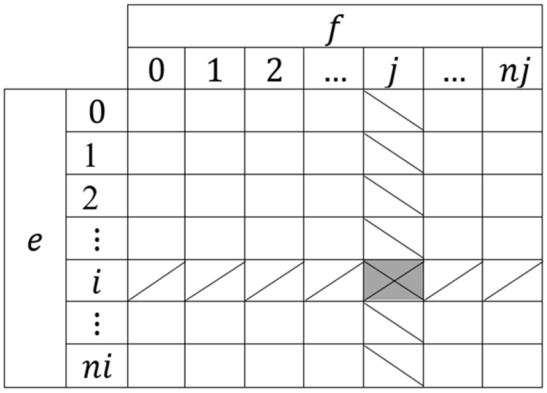

Figure A-1. Representation of the temperature discretisation (one element per domain)

Finally, we add a subscript to take the issue of the pipe into account. Then the temperature of each pipe k (k may be $p, p_r, in_{C_p}, out_{C_p}$) $T_k(t,x)$ is expressed with the use of the $ne \times (ni+1) \times nf \times (nj+1)$ coefficients $T_{k,e,i,f,j}$.

Then, applying the same methodology as for 1D-OCFE, we can approximate $\frac{\partial T_k}{\partial t}$ and $\frac{\partial T_k}{\partial x}$ as:

$$\begin{bmatrix} \left(\frac{\partial T_k}{\partial t}\right)_{e,1,f,j} \\ \left(\frac{\partial T_k}{\partial t}\right)_{e,2,f,j} \\ \vdots \\ \left(\frac{\partial T_k}{\partial t}\right)_{e,ni,f,j} \end{bmatrix} == \frac{1}{\Delta t_e} \cdot M_t \left(\begin{bmatrix} T_{k,e,1,f,j} \\ T_{k,e,2,f,j} \\ \vdots \\ T_{k,e,ni,f,j} \end{bmatrix} - \begin{bmatrix} T_{k,e,0,f,j} \\ T_{k,e,0,f,j} \\ \vdots \\ T_{k,e,0,f,j} \end{bmatrix} \right) = \begin{bmatrix} D_{t_1}(k,e,f,j) \\ D_{t_2}(k,e,f,j) \\ \vdots \\ D_{t_{ni-1}}(k,e,f,j) \end{bmatrix} \quad \text{(A-13)}$$

$$\begin{bmatrix} \left(\frac{\partial T_k}{\partial x}\right)_{e,i,f,1} \\ \left(\frac{\partial T_k}{\partial x}\right)_{e,i,f,2} \\ \vdots \\ \left(\frac{\partial T_k}{\partial x}\right)_{e,i,f,nj} \end{bmatrix} == \frac{1}{L_f} \cdot M_x \left(\begin{bmatrix} T_{k,e,i,f,1} \\ T_{k,e,i,f,2} \\ \vdots \\ T_{k,e,i,f,nj} \end{bmatrix} - \begin{bmatrix} T_{k,e,i,f,0} \\ T_{k,e,i,f,0} \\ \vdots \\ T_{k,e,i,f,0} \end{bmatrix} \right) = \begin{bmatrix} D_{x_1}(k,e,i,f) \\ D_{x_2}(k,e,i,f) \\ \vdots \\ D_{x_{nj-1}}(k,e,i,f) \end{bmatrix} \quad \text{(A-14)}$$

In equations (A-13) and (A-14) M_t and M_x represent the collocation matrices for the normalised domains with respective element sizes Δt_e and L_f. Finally, $D_{t_i}(k,e,f,j)$ and $D_{x_j}(k,e,i,f)$ denote the algebraic combinations to describe the variational terms.

For the first element on each domain, the values of the boundary conditions, $T_{k,1,0,f,j}$ and $T_{k,e,i,1,0}$, must be known. The way to achieve this will be explained in the next section. Then, for subsequent elements, these values correspond to those of the final point of the prior element. For the present application, we use the nodes of the shifted Legendre Gauss Lobatto quadrature as collocation points so that 0 and 1 are nodes.

Then for the other spatial-time points (other than $e,0,f,j$ and $e,i,f,0$) (e.g. $(\xi_j, \tau_i), j = 1 \dots nj, i = 1 \dots ni$)) we assume that equation (6) is satisfied. $T_k(\tau_i, \xi_j)$ is then replaced by $T_{k,e,i,f,j}$ and the derivatives are expressed by equations (A-13) and (A-14).

In Appendix B, we describe the implementation of 2D-OCFE to transform the heat equation into a set of algebraic equations, which, when coupled with the heat and mass balances, represent the dynamics of the DCS.

Appendix B. Discretised model

This appendix details the discretised model based on the equations presented in section 3.

B.1. Heat balances

As described in the previous section, 2D-OCFE will be applied to the PDE (6). To do this, the mass flow in each pipe, which is only time-dependent, also needs to be discretised as follows:

$$\dot{m}_k(\tau) = \sum_{i=0}^{ni} \dot{m}_{k,e,i}\, \ell_i(\tau) \tag{B-1}$$

The profile of the soil temperature $T_s(t)$ is known and corresponds to one of the profiles in section 2.3. When the PDE is applied in an element e in time at a collocation point τ_i we use the corresponding soil temperature which has been noted $T_{s,e,i}$.

$$T_{s,e,i} = T_s(\tau_i \Delta t_e + t_{e-1}) \tag{B-2}$$

In the same way, the temporal profile of the demand of each customer is known and we note:

$$Q_{C_p,e,i} = Q_{C_p}(\tau_i \Delta t_e + t_{e-1}) \tag{B-3}$$

As explained in the previous section, before applying orthogonal collocation, boundary conditions must be known, which will be explained later. Once these boundary conditions are known ($T_{k,1,0,f,j}$ $(j = 1 \dots nj)$ and $T_{k,e,i,1,0}$ $(i = 1, \dots ni)$), using equations (A-13) and (A-14), we can represent equation (6) for each pipe at each spatial-time point other than the boundary points, $(\tau_i, \xi_j), i = 1 \dots ni, j = 1 \dots nj$, by:

$$\rho_w \cdot Cp_w \cdot A_k \cdot D_{t_i}(k,e,f,j) + \dot{m}_{k,e,i} \cdot Cp_w \cdot D_{x_j}(k,e,i,f) = \frac{T_{s,e,i} - T_{k,e,i,f,j}}{R'} \tag{B-4}$$

By implementing this, we represent the PDE (6) as a set of $(ne \times ni \times nf \times nj)$ equations per pipe. The boundary conditions $T_{k,e,0,f,j}$ and $T_{k,e,i,f,0}$ are obtained from the configuration of the problem and from the heat and mass balances as follows:

- For elements $e > 1$ and $f > 1$, for each pipe, the initial conditions correspond to the final point of the previous one, as already stated.

$$T_{k,e,0,f,j} = T_{k,e-1,ni,f,j}\,, \quad e = 2 \dots ne\,, \quad f = 1 \dots nf\,, \quad j = 1 \dots nj \tag{B-5}$$

$$T_{k,e,i,f,0} = T_{k,e,i,f-1,nj}\,, \quad f = 2 \dots nf\,, \quad e = 1 \dots ne, \quad i = 1, \dots ni \tag{B-6}$$

and

$$T_{k,e,0,f,0} = T_{k,e-1,ni,f-1,nj}\ , \qquad e = 2 \dots ne\ , \qquad f = 2 \dots nf \tag{B-7}$$

- The element $e = 1$ equation (9) leads to the following $nf \times (nj + 1)$ equations in terms of discretised variables:

$$T_{k,1,0,f,j} = \theta_k\left(L_f \xi_j + x_{f-1}\right) = \theta_{k,f,j} \tag{B-8}$$

- For element $f = 1$, this condition depends on the pipe.
  - Equations (10) to (13) lead to the following: $ne \times (ni + 1) - 1$ equations in terms of discretised variables:

$$T_{0,e,i,1,0} = 277\ \text{K} \tag{B-9}$$

$$\begin{gathered} T_{p,e,i,nf,nj} = T_{p+1,e,i,1,0} = T_{in_{C_p},e,i,1,0}\ \ , p = 1 \dots 12{,}14, \dots 19 \\ T_{0,e,i,nf,nj} = T_{1,e,i,1,0} = T_{14,e,i,1,0} \\ T_{p,e,i,nf,nj} = T_{in_{C_p},e,i,1,0}\ \ ,\ \ p = 13\ , 20 \end{gathered} \tag{B-10}$$

$$\begin{gathered} \dot{m}_{p_r,e,i} \cdot T_{p_r,e,i,1,0} = \dot{m}_{p_r+1,e,i} \cdot T_{(p+1)_r,e,i,nf,nj} + \dot{m}_{out_{C_p},e,i} \cdot T_{out_{C_p},e,i,nf,nj}\ , \\ p = 1 \dots 12{,}14, \dots 19 \\ \dot{m}_{(0)_r,e,i} \cdot T_{(0)_r,e,i,1,0} = \dot{m}_{(1)_r,e,i} \cdot T_{(1)_r,e,i,nf,nj} + \dot{m}_{(14)_r,e,i} \cdot T_{(14)_r,e,i,nf,nj} \\ T_{(p)_r,e,i,1,0} = T_{out_{C_p},e,i,nf,nj}\ \ ,\ \ p = 13\ , 20 \end{gathered} \tag{B-11}$$

$$Q_{C_p,e,i} = \dot{m}_{in_{C_p},e,i} \cdot \mathrm{Cp}_w \cdot \left(T_{out_{C_p},e,i,1,0} - T_{in_{C_p},e,i,nf,nj}\right) \tag{B-12}$$

Finally, Figure B-1 summarises variables $T_{k,e,i,f,j}$ and their associated equations.

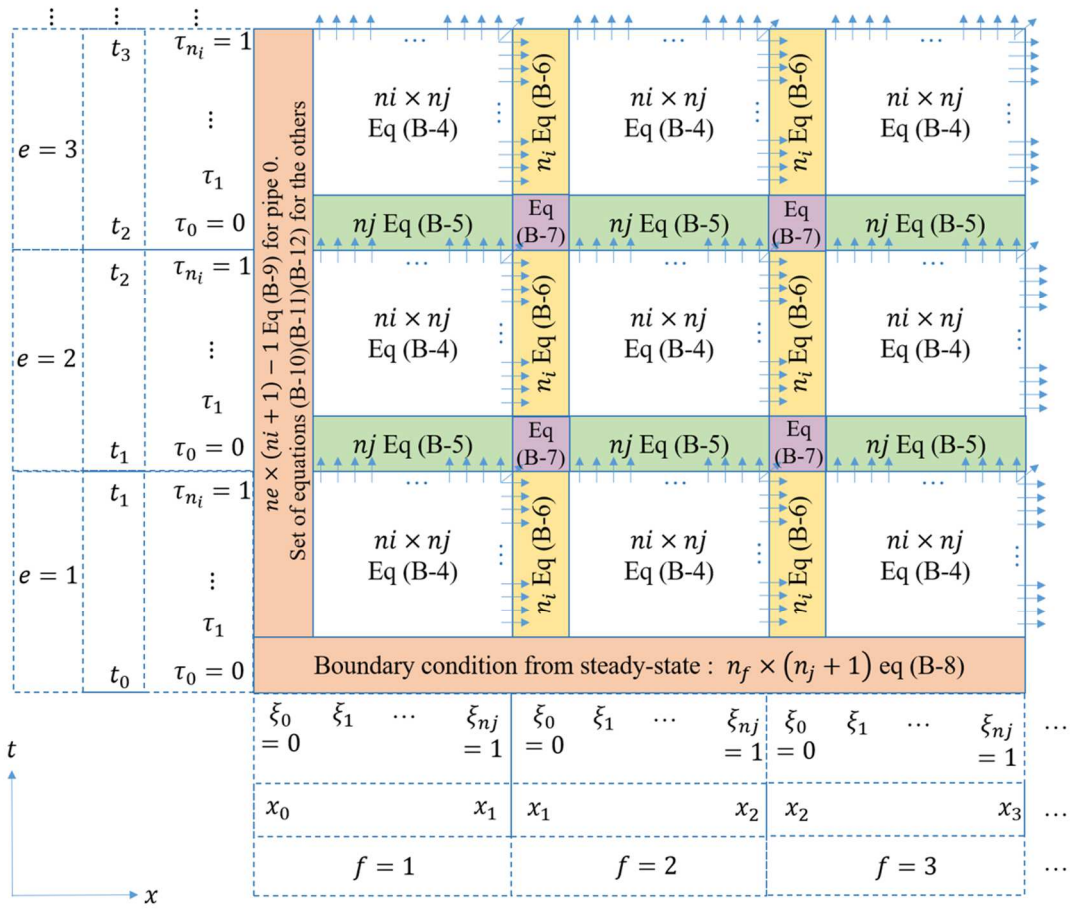

Figure B-1. Associated equations for the solution of the PDE on a pipe

B.2. Mass balances

In this section, the mass balance equations and the constraints concerning the velocity and the flow policy involve only time-dependent variables. Therefore, each of these equations from the original PDAE problem leads to a corresponding set of $ne \times (ni + 1)$ equations, replacing $\dot{m}_k(t)$ and $v_k(t)$ by $\dot{m}_{k,e,i}$ and $v_{k,e,i}$. In this section, these equations are written in terms of discretised variables.

Mass balance equations (14), (15) and (16) lead to:

$$\dot{m}_{p,e,i} = \dot{m}_{p+1,e,i} + \dot{m}_{in_{C_p},e,i} \quad p = 1 \dots 12,14 \dots 19$$

$$\dot{m}_{p,e,i} = \dot{m}_{in_{C_p},e,i} \quad p = 13\,,20 \qquad \text{(B-13)}$$

$$\dot{m}_{0,e,i} = \dot{m}_{1,e,i} + \dot{m}_{14,e,i}$$

$$\dot{m}_{p_r,e,i} = \dot{m}_{(p+1)_r,e,i} + \dot{m}_{out_{C_p},e,i} \quad p = 1 \dots 12,14 \dots 19$$

$$\dot{m}_{p_r,e,i} = \dot{m}_{out_{C_p},e,i} \quad p = 13\,,20 \qquad \text{(B-14)}$$

$$\dot{m}_{0_r,e,i} = \dot{m}_{1_r,e,i} + \dot{m}_{14_r,e,i}$$

$$\dot{m}_{in_{C_p},e,i} = \dot{m}_{out_{C_p},e,i} \quad p = 1 \dots 20 \tag{B-15}$$

Flow policy equations (17) and (18) lead to:

$$\dot{m}_{0,e,i} = \dot{m}_{0\mathrm{Cte}} \tag{B-16}$$

$$\frac{Peak(1)}{\dot{m}_{in_{C_1},e,i}} = \frac{Peak(p)}{\dot{m}_{in_{C_p},e,i}}, \quad \forall\, p \in \{2, \dots, 20\} \tag{B-17}$$

and the flow velocity equation (20) leads to:

$$v_{k,e,i} \leq v_{max,k} \tag{B-18}$$

Finally, the $n_{pipes} \times n_e \times (n_i + 1)$ variables $\dot{m}_{k,e,i}$, with $n_{pipes} = 82$, are associated with:

$21 \times n_e \times (n_i + 1)$ equations (B-13).

$21 \times n_e \times (n_i + 1)$ equations (B-14).

$20 \times n_e \times (n_i + 1)$ equations (B-15).

$1 \times n_e \times (n_i + 1)$ equations (B-16).

$19 \times n_e \times (n_i + 1)$ equations (B-17).

Together with the variables $T_{k,e,i,f,j}$ associated with the equations described in the previous section, they constitute the algebraic system that must be solved.

The set of equations (B-4) to (B-18) results from the implementation of 2D-OCFE in the original PDAE problem. This formulation will allow us to perform the dynamic simulation analysis of the case study, whose main output will be the temperature profiles of the pipes that make up the system.

Appendix C. Validation of the discretization method

To validate the proposed 2D-OCFE method for solving the dynamic one-dimensional heat transfer equation in pipes, we analyse a simple case study. The problem is solved using a well- known discretisation strategy (second-order centred finite differences for time and space) as a reference scenario, which will be compared to the solution obtained via 2D-OCFE.

We propose to study the propagation of a temperature wave in the inlet of a 12-inch non-insulated pipe with a length of 1km, a constant flow velocity of 0.97m/s, and external temperature (T_s) varying linearly from 25°C to 27°C, for 1 hour.

First, we defined the number of discretisation points for the reference scenario. For this, we made several runs by incrementing the number of points on each domain (x, t) and comparing the results from each run until the change in the computed values was negligible. Next, we chose a reference scenario computed with 1200 discrete points in time and 200 in distance using the method of second-order centred finite differences. The computational time for this scenario was 24.84 s.

Then we implemented the proposed 2D-OCFE method to solve this problem using different combinations of the number of elements (ne and nf) and collocation points ($(ni + 1)$ and $(nj + 1)$) on each domain, and comparing each result with the reference scenario. Table C-1 details some of the implemented combinations, their corresponding % of error with respect to the reference scenario and the computational time.

Table C-1. 2D-OCFE combinations results

ne	ni+1	nf	$nj + 1$	Error [%]	CPU time (s)
30	6	2	6	[-0.0056, 0.0044]	0.047
30	6	3	6	[-0.0027,0.0054]	0.047
30	6	4	6	[-0.0049, 0.0056]	0.062
30	6	5	6	[-0.0028, 0.0052]	0.094

We can see that via 2D-OCFE the number of points required is considerably reduced, from 1200 to 180 in time and from 200 to 30 (at most) in distance, achieving accurate results with respect to the reference scenario, given the reported errors, with computational times more than 250 times smaller than implementing a conventional discretisation strategy.

Finally, Figure C-1 shows the inlet temperature wave and the variation in temperature at the pipe outlet for some of the runs made to define the reference scenario (1200 t) using 200 discretisation points in distance. These are compared to the response using 2D-OCFE (last case in Figure C-1)Here, we show that by using 2D-OCFE it is possible to compute more accurate results than with some conventional discretisation using 150 and 500 points in time.

These results validate the accuracy of the proposed 2D-OCFE, and thus we can replicate it for the analysis of district cooling systems.

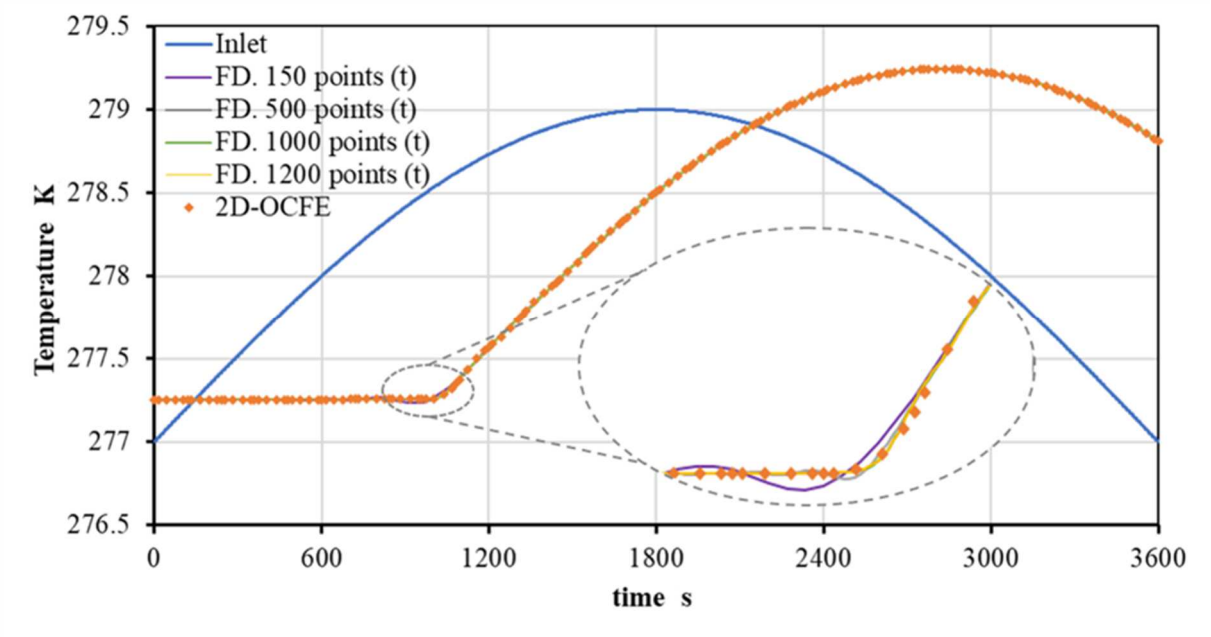

Figure C-1. Pipe inlet temperature variation and comparison of outlet responses

Nomenclature

Symbols

	$\bar{h}$	Convective heat transfer coefficient, $Wm^{-2}K^{-1}$
	Cp	Specific Heat Capacity, $J\ kg^{-1}K^{-1}$
	L	Pipe length, m
	L_f	Length of spatial finite element
	$\dot{m}$	Mass flow rate, $kg\ s^{-1}$
	N_x	Spatial collocation matrix
	N_x	Temporal collocation matrix
	r	radius, m
	R'	Total thermal resistance, $m\ K\ W^{-1}$
	t	Time, s
	T	Temperature, K
	v	Velocity, $m\ s^{-1}$
	ΔT	Temperature difference, K
	Δt_e	Size of temporal finite element

Greek symbols

	λ	Conductivity, $W\ m^{-1}\ K^{-1}$
	ρ	Density, $kg\ m^{-3}$
	ξ	Normalised spatial variable
	τ	Normalised time variable

θ Steady-state temperature

Sets and indices

C_p Set of consumers

D_{t_i} Linear transformation for time derivative

D_{x_j} Linear transformation for space derivative

e Index for time elements

f Index for distance elements

i Index for time collocation points in time

j Index for distance collocation points

k Index of pipes

p Sub-index for main pipes

in_{Cp} Sub-index for pipes entering clients

out_{Cp} Sub-index for pipes leaving clients

Subscripts

r Return pipe

s Soil

w Water

References

[1] Möller B, Wiechers E, Persson U, Grundahl L, Connolly D. Heat Roadmap Europe: Identifying local heat demand and supply areas with a European thermal atlas. Energy 2018;158:281–92. DOI:10.1016/j.energy.2018.06.025.

[2] Pacesila M, Burcea SG, Colesca SE. Analysis of renewable energies in European Union. Renew Sustain Energy Rev 2016;56:156–70. DOI:10.1016/j.rser.2015.10.152.

[3] Lake A, Rezaie B, Beyerlein S. Review of district heating and cooling systems for a sustainable future. Renew Sustain Energy Rev 2017;67:417–25. DOI:10.1016/j.rser.2016.09.061.

[4] Sameti M, Haghighat F. Optimization approaches in district heating and cooling thermal network. Energy Build 2017;140:121–30. DOI:10.1016/j.enbuild.2017.01.062.

[5] Werner S. International review of district heating and cooling. Energy 2017;137:617–31. DOI:10.1016/j.energy.2017.04.045.

[6] Biegler LT, Grossmann IE. Retrospective on optimization. Comput Chem Eng 2004;28:1169–92. DOI:10.1016/j.compchemeng.2003.11.003.

[7] Talebi B, Mirzaei PA, Bastani A, Haghighat F. A Review of District Heating Systems: Modeling and Optimization. Front Built Environ 2016;2. DOI:10.3389/fbuil.2016.00022.

[8] Gang W, Wang S, Xiao F, Gao D. District cooling systems: Technology integration, system optimization, challenges and opportunities for applications. Renew Sustain Energy Rev 2016;53:253–64. DOI:10.1016/j.rser.2015.08.051.

[9] Eveloy V, Ayou DS. Sustainable District Cooling Systems: Status, Challenges, and Future Opportunities, with Emphasis on Cooling-Dominated Regions. Energies 2019;12:235. DOI:10.3390/en12020235.

[10] Allegrini J, Orehounig K, Mavromatidis G, Ruesch F, Dorer V, Evins R. A review of modelling approaches and tools for the simulation of district-scale energy systems. Renew Sustain Energy Rev 2015;52:1391–404. DOI:10.1016/j.rser.2015.07.123.
[11] Chow TT, Chan ALS, Song CL. Building-mix optimization in district cooling system implementation. Appl Energy 2004;77:1–13. DOI:10.1016/S0306-2619(03)00102-8.
[12] Deng N, Cai R, Gao Y, Zhou Z, He G, Liu D, et al. A MINLP model of optimal scheduling for a district heating and cooling system: A case study of an energy station in Tianjin. Energy 2017;141:1750–63. DOI:10.1016/j.energy.2017.10.130.
[13] Söderman J. Optimisation of structure and operation of district cooling networks in urban regions. Appl Therm Eng 2007;27:2665–76. DOI:10.1016/j.applthermaleng.2007.05.004.
[14] Mertz T, Serra S, Henon A, Reneaume J-M. A MINLP optimization of the configuration and the design of a district heating network: Academic study cases. Energy n.d. DOI:10.1016/j.energy.2016.07.106.
[15] Marty F, Serra S, Sochard S, Reneaume J-M. Simultaneous optimization of the district heating network topology and the Organic Rankine Cycle sizing of a geothermal plant. Energy 2018;159:1060–74. DOI:10.1016/j.energy.2018.05.110.
[16] Khir R, Haouari M. Optimization models for a single-plant District Cooling System. Eur J Oper Res 2015;247:648–58. DOI:10.1016/j.ejor.2015.05.083.
[17] Schweiger G, Larsson P-O, Magnusson F, Lauenburg P, Velut S. District heating and cooling systems – Framework for Modelica-based simulation and dynamic optimization. Energy 2017;137:566–78. DOI:10.1016/j.energy.2017.05.115.
[18] Powell KM, Hedengren JD, Edgar TF. Dynamic optimization of a hybrid solar thermal and fossil fuel system. Sol Energy 2014;108:210–8. DOI:10.1016/j.solener.2014.07.004.
[19] Longuski JM, Guzmán JJ, Prussing JE. Optimal Control with Aerospace Applications. New York: Springer-Verlag; 2014.
[20] Biegler LT. Nonlinear programming strategies for dynamic chemical process optimization. Theor Found Chem Eng 2014;48:541–54. DOI:10.1134/S0040579514050157.
[21] Biegler LT. Advanced optimization strategies for integrated dynamic process operations. Comput Chem Eng 2018;114:3–13. DOI:10.1016/j.compchemeng.2017.10.016.
[22] Hedengren JD, Shishavan RA, Powell KM, Edgar TF. Nonlinear modeling, estimation and predictive control in APMonitor. Comput Chem Eng 2014;70:133–48. DOI:10.1016/j.compchemeng.2014.04.013.
[23] Esche E, Arellano-Garcia H, Wozny G, Biegler LT. Optimal Operation of a Membrane Reactor Network. In: Karimi IA, Srinivasan R, editors. Comput. Aided Chem. Eng., vol. 31, Elsevier; 2012, p. 1321–5. DOI:10.1016/B978-0-444-59506-5.50095-X.
[24] Jacobsen LT, Spivey BJ, Hedengren JD. Model predictive control with a rigorous model of a Solid Oxide Fuel Cell. 2013 Am. Control Conf., 2013, p. 3741–6. DOI:10.1109/ACC.2013.6580409.
[25] Mittal AK, Ganaie IA, Kukreja VK, Parumasur N, Singh P. Solution of diffusion–dispersion models using a computationally efficient technique of orthogonal collocation on finite elements with cubic Hermite as basis. Comput Chem Eng 2013;58:203–10. DOI:10.1016/j.compchemeng.2013.07.007.
[26] Branan CR. 1 - Fluid Flow. Rules Thumb Chem. Eng. Fourth Ed., Burlington: Gulf Professional Publishing; 2005, p. 2–28. DOI:10.1016/B978-075067856-8/50001-3.
[27] Olama AA. District Cooling: Theory and Practice. 1 edition. Boca Raton: CRC Press; 2016.
[28] Phetteplace G, Abdullah S, Bahnfleth D, Meyer V, Andrepont J, Ghani A, et al. District Cooling Guide. Atlanta, GA: ASHRAE; 2013.
[29] Weather Forecast & Reports - Long Range & Local. Weather Undergr n.d. / (accessed December 7, 2018).
[30] Oppelt T, Urbaneck T, Gross U, Platzer B. Dynamic thermo-hydraulic model of district cooling networks. Appl Therm Eng 2016;102:336–45. DOI:10.1016/j.applthermaleng.2016.03.168.
[31] Duquette J, Rowe A, Wild P. Thermal performance of a steady state physical pipe model for simulating district heating grids with variable flow. Appl Energy 2016;178:383–93.

[32] van der Heijde B, Fuchs M, Ribas Tugores C, Schweiger G, Sartor K, Basciotti D, et al. Dynamic equation-based thermo-hydraulic pipe model for district heating and cooling systems. Energy Convers Manag 2017;151:158–69. DOI:10.1016/j.enconman.2017.08.072.
[33] Bergman TL, Incropera FP. Fundamentals of Heat and Mass Transfer. John Wiley & Sons; 2011.
[34] Winterton RHS. Where did the Dittus and Boelter equation come from? Int J Heat Mass Transf 1998;41:809–10. DOI:10.1016/S0017-9310(97)00177-4.
[35] Greyvenstein GP. An implicit method for the analysis of transient flows in pipe networks. Int J Numer Methods Eng 2002;53:1127–43. DOI:10.1002/nme.323.
[36] Gabrielaitienė I, Kačianauskas R, Sunden B. Thermo-Hydraulic Finite Element Modelling of District Heating Network by the Uncoupled Approach. J Civ Eng Manag 2003;9:153–62. DOI:10.1080/13923730.2003.10531321.
[37] Ben Hassine I, Eicker U. Impact of load structure variation and solar thermal energy integration on an existing district heating network. Appl Therm Eng 2013;50:1437–46. DOI:10.1016/j.applthermaleng.2011.12.037.
[38] Zhou S, Tian M, Zhao Y, Guo M. Dynamic modeling of thermal conditions for hot-water district-heating networks. J Hydrodyn Ser B 2014;26:531–7. DOI:10.1016/S1001-6058(14)60060-3.
[39] Stevanovic VD, Zivkovic B, Prica S, Maslovaric B, Karamarkovic V, Trkulja V. Prediction of thermal transients in district heating systems. Energy Convers Manag 2009;50:2167–73. DOI:10.1016/j.enconman.2009.04.034.
[40] Finlayson BA. Orthogonal Collocation in Chemical Reaction Engineering. Catal Rev 1974;10:69–138. DOI:10.1080/01614947408079627.
[41] Ebrahimzadeh E, Shahrak MN, Bazooyar B. Simulation of transient gas flow using the orthogonal collocation method. Chem Eng Res Des 2012;90:1701–10. DOI:10.1016/j.cherd.2012.02.018.
[42] Biegler LT. Nonlinear Programming: Concepts, Algorithms, and Applications to Chemical Processes. SIAM-Society for Industrial and Applied Mathematics; 2010.
[43] Agency IE. District heating and cooling connection handbook. Sittard: Netherlands Agency for Energy and the Environment; 2002.
[44] Safdarnejad SM, Hedengren JD, Lewis NR, Haseltine EL. Initialization strategies for optimization of dynamic systems. Comput Chem Eng 2015;78:39–50. DOI:10.1016/j.compchemeng.2015.04.016.
[45] North American Insulation Manufacturers Association (NAIMA). Guide to Insulating Chilled Water Systems with Mineral Fiber Pipe Insulation. First Edition. Alexandria, VA 22314: North American Insulation Manufacturers Association (NAIMA); 2015.
[46] Lo A. Optimizing the cost and energy performance of district cooling system with the low delta-T syndrome. phd. Cardiff University, 2014.
[47] American Society of Heating R and A-CE. 2013 ASHRAE handbook: fundamentals. 2013.
[48] Hyman LB, Phetteplace G, Tredinnick S. District Heating and Cooling. Ashrae Handb. 2016 HVAC Syst. Equip. SI Ed., ASHRAE; 2016.
[49] Canuto C, Hussaini MY, Quarteroni A, Zang TA. Spectral Approximation. In: Canuto C, Hussaini MY, Quarteroni A, Zang TA, editors. Spectr. Methods Fluid Dyn., Berlin, Heidelberg: Springer Berlin Heidelberg; 1988, p. 31–75. DOI:10.1007/978-3-642-84108-8_2.
[50] Surjanhata H. On orthogonal collocation solutions of partial differential equations. Ph.D. Thesis. New Jersey Institute of Technology, 1993.